Quantitative Robust Control Engineering: Theory and Applications

Mario Garcia-Sanz
Automatic Control and Computer Science Department
Public University of Navarra. Campus Arrosadia
31006 Pamplona
SPAIN

E-mail: mgsanz@unavarra.es

ABSTRACT

This paper presents a summary of the main concepts and references of the Quantitative Feedback Theory (QFT). It is a frequency domain engineering method to design robust controllers. It explicitly emphasises the use of feedback to simultaneously reduce the effects of model plant uncertainty and to satisfy performance specifications. QFT highlights the trade-off (quantification) among the simplicity of the controller structure, the minimization of the 'cost of feedback', the existing model uncertainty and the achievement of the desired performance specifications at every frequency of interest. The technique has been successfully applied to control a wide variety of physical systems. After a brief introduction about the essential aspects of the QFT design methodology, including a wide set of QFT references, this paper presents a new method to extend the classical diagonal QFT controller design method for MIMO plants with model uncertainty to a fully populated matrix controller design method. The paper simultaneously studies three cases: the reference tracking, the external disturbance rejection at plant input and the external disturbance rejection at plant output. The work ends showing several real-world examples where the controllers have been designed using QFT techniques: an industrial SCARA robot manipulator, a wastewater treatment plant, a variable speed wind turbine of 1.65 MW and an industrial furnace of 1 MW.

1.0 INTRODUCTION

Much of the current interest in frequency domain robust stability and robust performance dates from the original works of H.W. Bode (1945) [1] and I. Horowitz (1963) [2]. Since then, and during the entire second half of the twentieth century, there has been a tremendous advance in the state-of-the-art of robust frequency domain methods. One of the main techniques, introduced by Prof. Isaac Horowitz in 1959 [24], which characterises closed loop performance specifications against parametric plant uncertainty, mapped into open loop design constraints, became known as Quantitative Feedback Theory (QFT) in the seventies [25-27]. This paper presents a summary of the main ideas and references of the QFT methodology.

The method searches for a controller that guarantees the achievement of the desired performance specifications for every plant within the existing model uncertainty. QFT highlights the trade-off (*quantification*) among the simplicity of the controller structure, the minimization of the 'cost of feedback' (*bandwidth*), the model uncertainty (*parametric and non-parametric*) and the achievement of the desired performance specifications at every frequency of interest.

Following this introduction, Section 2 presents a brief description of the essential aspects of the QFT methodology. Section 3 introduces a method to design non-diagonal QFT controllers for MIMO systems. Afterwards the paper describes some real-world applications of the technique, carried out by the author: an

Garcia-Sanz, M. (2006) Quantitative Robust Control Engineering: Theory and Applications. In *Achieving Successful Robust Integrated Control System Designs for 21st Century Military Applications – Part II* (pp. 1-1 – 1-44). Educational Notes RTO-EN-SCI-166, Paper 1. Neuilly-sur-Seine, France: RTO. Available from: http://www.rto.nato.int/abstracts.asp.

industrial SCARA robot manipulator in Section 4, a wastewater treatment plant of 5000 m^3/hour in Section 5, a variable speed wind turbine of 1.65 MW in Section 6 and an industrial furnace of 40 metres and 1 MW in Section 7. The paper ends with a wide References Section that includes a representative collection of books and papers related with the theory and applications of QFT.

2.0 QUANTITATIVE FEEDBACK THEORY

The Quantitative Feedback Theory (QFT), first introduced by Prof. Isaac Horowitz in 1959 [24], is an engineering method, which explicitly emphasises the use of feedback to simultaneously reduce the effects of plant uncertainty and satisfy performance specifications. Horowitz's work is deeply rooted in classical frequency response analysis involving Bode diagrams, template manipulations and Nichols Charts (NC). It relies on the observation that the feedback is needed principally when the plant presents model uncertainty or when there are uncertain disturbances acting on the plant.

Frequency domain specifications and desired time-domain responses translated into frequency domain tolerances, lead to the so-called Horowitz-Sidi bounds (or constraints). These bounds serve as a guide for shaping the nominal loop transfer function $L(s) = G(s)\,P(s)$, which involves the manipulation of gain, poles and zeros on the controller $G(s)$. On the whole, the QFT main objective is to synthesize (loop-shape) a simple, low-order controller with minimum bandwidth, which satisfies the desired specifications and tackles feedback control problems with robust performance objectives.

In the last few decades QFT has been successfully applied to many control problems. A wide collection of books and papers about the main aspects of the QFT methodology, theory and applications, is included in the references section: controller loop-shaping [41-44], existence conditions for controllers [45-47], multi-input multi-output MIMO systems [48-63], time-delay systems [64], digital QFT [65-66], distributed parameter systems [67-74], non-minimum phase systems [75-80], multi-loop systems [81-83], non-linear systems [84-92], linear time variant systems LTV [93-94], QFT software packages [95-102], real-world applications [103,127].

A detailed study about the history of QFT can be found in the papers written by Horowitz [19-21], Houpis [22] and Garcia-Sanz [23]. In 1992, Houpis and Chandler organized in Wright-Patterson (Dayton, Ohio) the first International QFT Symposium [10]. Since then, and with the continuous support of Prof. Houpis, the Symposia have been organized every two years: Indiana-USA-1995 [11], Glasgow-UK-1997 [12], Durban - South Africa - 1999 [13], Pamplona-Spain-2001 [14], and Cape Town - South Africa -2003 [15]. The next one will be in Kansas-USA-2005.

To go into the QFT theoretical aspects in depth, check the excellent tutorials written by Horowitz [16-17] and Houpis [18]. In addition, a major analysis can be found in the books written by Horowitz [3], Houpis, Rasmussen and Garcia-Sanz [4], Yaniv [5] and Sidi [6]. Finally, three special issues of the *International Journal of Robust and Nonlinear Control* (*Wiley*) describe some of the more significant advances of QFT: Houpis 1997 [7], Eitelberg 2001-2002 [8] and Garcia-Sanz 2003 [9].

The QFT design methodology is quite transparent, allowing the designer to see the necessary trade-offs to achieve the closed-loop system specifications. The basic steps of the procedure (see also Fig. 4) are presented in the following sub-sections. They are:

- Plant model (with uncertainty), Templates generation and nominal plant selection $P_o(j\omega)$.
- Performance Specifications.
- QFT Bounds $B(j\omega)$.
- Loop-shaping the controller $G(j\omega)$.
- Pre-filter synthesis $F(j\omega)$.
- Simulation and Design Validation.

2.1 Plant Model and Templates Generation

The plant dynamics to be controlled may be described by frequency response data, or by linear or nonlinear transfer functions with mixed (parametric and non-parametric) uncertainty models. It can be defined taking into account the parameter uncertainty of the process at every frequency of interest (ω_i), that is to say the plant uncertainty templates, so that $\Im P(j\omega_i)=\{P(j\omega_i),\ \omega_i \in \cup\Omega_k\}$.

The templates are sets of complex numbers representing the frequency response of the family of uncertain plants at a fixed frequency $\Im P(j\omega_i)$, i.e. a template is a projection of the *n*-dimensional parameter space onto the Nichols Chart. Fig.1 represents the QFT-template of the plant $P(s) = \exp(-\tau s)/(s^2 + 2\zeta\,\omega_n\, s + \omega_n^2)$ with three parameters, two with uncertainty ($\zeta = 0.02$, $\omega_n = [0.7, 1.2]$, $\tau = [0, 2]$), at $\omega = 1$ rad/s. For more information about the QFT templates see [28-34].

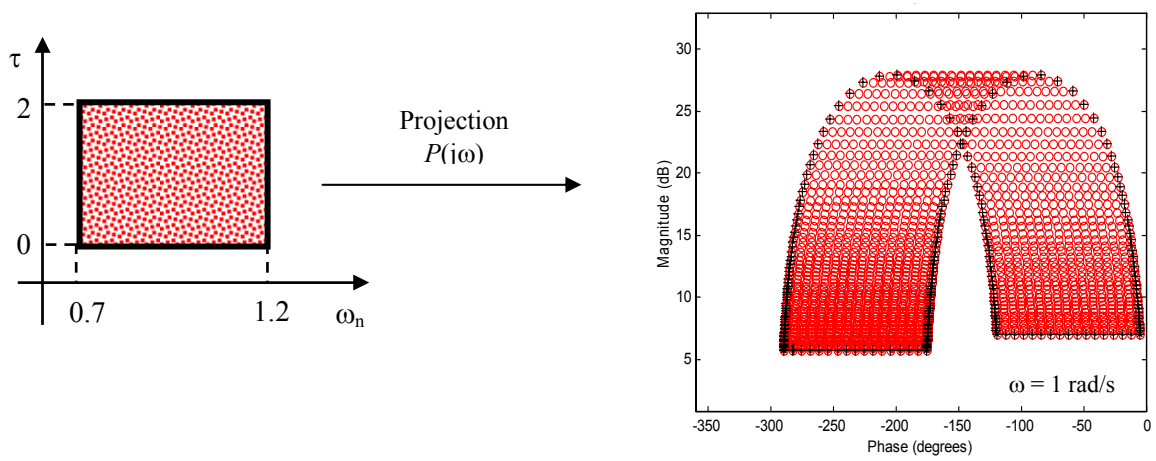

Figure 1: Template of the plant at ω = 1 rad/s

2.2 Performance specifications

The standard two degree of freedom system which best exemplifies the feedback problem considered in QFT is shown in Fig. 2. It includes the set of uncertain plants, -$\Im P(j\omega_i)=\{P(j\omega_i),\ \omega_i \in \cup\Omega_k\}$-, the loop controller -*G*- and the pre-filter -*F*-, both to be design, and the sensor dynamics -*H*-. On the other hand, *R*, *E*, *U*, *Y* and *N* are vectors representing respectively: the reference input, the error signal, the controller output, the plant output and the sensor noise input. *W*, D_1 and D_2 are the external disturbance inputs. From the structure we can define the Eqs. (1) to (3),

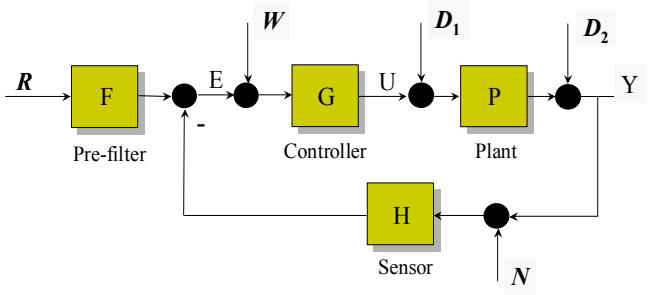

Figure 2: Standard two-degree-of-freedom feedback structure

$$Y = \frac{1}{1+PGH} D_2 + \frac{P}{1+PGH} D_1 + \\ + \frac{PG}{1+PGH}(W + FR) - \frac{PGH}{1+PGH} N \quad \textbf{(1)}$$

$$U = \frac{G}{1+PGH}(W + FR) - \frac{GH}{1+PGH}(N + D_2 + PD_1) \quad \textbf{(2)}$$

$$E = -\frac{H}{1+PGH} D_2 + \frac{PH}{1+PGH} D_1 + \frac{PGH}{1+PGH} W + \\ + \frac{1}{1+PGH} FR - \frac{H}{1+PGH} N \quad \textbf{(3)}$$

Table I. Transfer functions and specification models (H=1)	*No.Eq.*
$\lvert T_1(j\omega)\rvert = \left\lvert \frac{Y(j\omega)}{R(j\omega)F(j\omega)} \right\rvert = \left\lvert \frac{U(j\omega)}{D_1(j\omega)} \right\rvert = \left\lvert \frac{Y(j\omega)}{N(j\omega)} \right\rvert = \left\lvert \frac{P(j\omega)\,G(j\omega)}{1+P(j\omega)\,G(j\omega)} \right\rvert \le \delta_1(\omega), \quad \omega \in \Omega_1$	**(4)**
$\lvert T_2(j\omega)\rvert = \left\lvert \frac{Y(j\omega)}{D_2(j\omega)} \right\rvert = \left\lvert \frac{1}{1+P(j\omega)\,G(j\omega)} \right\rvert \le \delta_2(\omega), \quad \omega \in \Omega_2$	**(5)**
$\lvert T_3(j\omega)\rvert = \left\lvert \frac{Y(j\omega)}{D_1(j\omega)} \right\rvert = \left\lvert \frac{P(j\omega)}{1+P(j\omega)G(j\omega)} \right\rvert \le \delta_3(\omega), \quad \omega \in \Omega_3$	**(6)**
$\lvert T_4(j\omega)\rvert = \left\lvert \frac{U(j\omega)}{D_2(j\omega)} \right\rvert = \left\lvert \frac{U(j\omega)}{N(j\omega)} \right\rvert = \left\lvert \frac{U(j\omega)}{R(j\omega)\,F(j\omega)} \right\rvert = \left\lvert \frac{G(j\omega)}{1+P(j\omega)\,G(j\omega)} \right\rvert \le \delta_4(\omega), \quad \omega \in \Omega_4$	**(7)**
$\delta_{5\inf}(\omega) < \lvert T_5(j\omega)\rvert = \left\lvert \frac{Y(j\omega)}{R(j\omega)} \right\rvert = \left\lvert F(j\omega)\,\frac{P(j\omega)\,G(j\omega)}{1+P(j\omega)\,G(j\omega)} \right\rvert \le \delta_{5\sup}(\omega), \quad \omega \in \Omega_5$	**(8)**
$\frac{\lvert G(j\omega)P_d(j\omega)\rvert}{\lvert G(j\omega)P_e(j\omega)\rvert} \frac{\lvert 1+G(j\omega)P_e(j\omega)\rvert}{\lvert 1+G(j\omega)P_d(j\omega)\rvert} \le \delta_5(\omega) = \frac{\delta_{5\,sup}(\omega)}{\delta_{5\,inf}(\omega)}, \quad \omega \in \Omega_5$	**(9)**

To achieve reliability and robustness, QFT deals with robust stability margins and robust performance specifications (disturbance rejection, reference tracking, etc) as objectives in terms of the transfer functions of Eqs. (1) to (3) over the frequencies of interest (Table I).

2.3 QFT-bounds

For a nominal plant $P_0(j\omega)$, member of the family of plants within the uncertainty $\Im P(j\omega)$, the QFT methodology converts closed-loop system specifications and model plant uncertainty in a set of constrains or bounds (Horowitz-Sidi Bounds) for every frequency of interest that will have to be fulfilled by the nominal open-loop transfer function. They are represented on a Nichols chart. Such a great integration of information in a set of simple curves (the bounds) will allow designing the controller using only a single plant, the nominal plant P_0.

The ω_i plant template, $\Im P(j\omega_i) = \{P(j\omega_i)\}$, is approximated by a finite set of boundary plants $\{P_r(j\omega_i)$, r = 1,...,m$\}$. Each plant can be expressed in its polar form as $P_r(j\omega_i) = p(\omega_i)\, e^{j\theta}\ (\omega_i) = p\angle\theta$, and likewise the

controller polar form is $G(j\omega_i) = g(\omega_i)\, e^{j\phi} = g\angle\phi$. The controller phase ϕ varies from -2π to 0. Therefore, for every frequency ω_i, the feedback specifications $\{|T_k(j\omega_i)| \le \delta_k(\omega_i),\ k=1,...,5\}$ in Table I –Eqs. (4) to (9)- are translated into the quadratic inequalities in Table II –Eqs. (10) to (14)-, see [16].

k	Table II. Quadratic inequality on g	*Eq.*
1	$p^2\left(1-\frac{1}{\delta_1^2}\right)g^2 + 2\,p\cos(\phi+\theta)\,g + 1 \ge 0$	**(10)**
2	$p^2\,g^2 + 2\,p\cos(\phi+\theta)\,g + \left(1-\frac{1}{\delta_2^2}\right) \ge 0$	**(11)**
3	$p^2\,g^2 + 2\,p\cos(\phi+\theta)\,g + \left(1-\frac{p^2}{\delta_3^2}\right) \ge 0$	**(12)**
4	$\left(p^2-\frac{1}{\delta_4^2}\right)g^2 + 2\,p\cos(\phi+\theta)\,g + 1 \ge 0$	**(13)**
5	$p_e^2 p_d^2\left(1-\frac{1}{\delta_5^2}\right)g^2 + 2p_e\,p_d\left(p_e\cos(\phi+\theta_d) - \frac{p_d}{\delta_5^2}\cos(\phi+\theta_e)\right)g + \left(p_e^2-\frac{p_d^2}{\delta_5^2}\right) \ge 0$	**(14)**

The format of these quadratic expressions is:

$$I_{\omega_i}^k(p,\theta,\delta_k,\phi) = a\,g^2 + b\,g + c \ge 0 \qquad \textbf{(15)}$$

Chait and Yaniv [35] developed an algorithm to compute the bounds based on quadratic inequalities (see Table II), simplifying much of the work on traditional manual bound computation. Taking these inequalities into account, it is possible to compute them at the NC. Once the bounds have been calculated for the performance specifications, they have to be grouped into a single variable.

Then, the worst case bound, i.e. the most restrictive one for every phase, is computed for each frequency of the work array (see Figure 3). For more information about the QFT bounds see [35-40].

2.4 Controller design

In the design stage (loop-shaping), the controller $G(s)$ is synthesized on the NC by adding poles and zeros until the nominal loop, defined as $L_0 = P_0\, G$, lies near its bounds. Loop-shaping considers bounds on the NC to express the plant model with uncertainty and the performance specifications at every frequency.

An optimal controller will be obtained if it meets its bounds (over the continuous lines and under the dashed lines at every frequency) and it has the minimum high frequency gain (see Fig.3).

Although current CAD tools for QFT controller design are very helpful [95-102], the loop-shaping step must be still done manually using designer skills and experience. Even keeping the controller structure fixed, automatic tuning of parameters represents a great challenge [43-44].

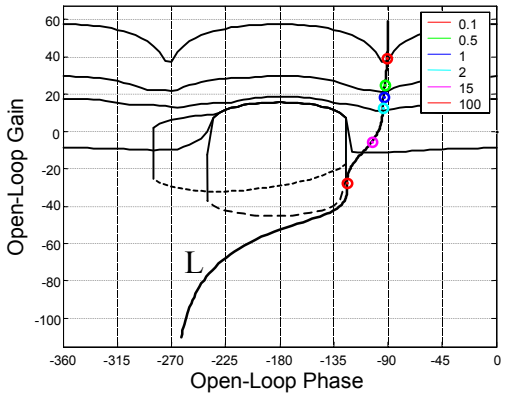

Figure 3: Loop shaping

The general formulation for the controller structure is expressed by the following transfer function:

$$G(s) = k_G \frac{\prod_{i=1}^{n_{rz}} \left(\frac{s}{z_i} + 1 \right) \prod_{i=1}^{n_{cz}/2} \left(\frac{s^2}{|z_i|^2} + \frac{2\,\mathrm{Re}(z_i)}{|z_i|^2} s + 1 \right)}{s^r \prod_{j=1}^{m_{rp}} \left(\frac{s}{p_j} + 1 \right) \prod_{j=1}^{m_{cp}/2} \left(\frac{s^2}{|p_j|^2} + \frac{2\,\mathrm{Re}(p_j)}{|p_j|^2} s + 1 \right)} \tag{16}$$

where, k_G is the gain, z_i is a zero that may be complex (n_{cz}, number of complex zeros) or real (n_{rz}, number of real zeros), and p_j is a pole (real or complex) with m_{rp} the number of real poles and m_{cp} the number of complex poles. Note that the amount of complex zeros or poles must be even, to have pairs of complex conjugate numbers and obtain a polynomial with real coefficients. Controller may have some poles in the origin and designer can check the parameter r (usually 0, 1 or 2) to set them. For more information about QFT loop-shaping see [41-44], and about existence conditions for controllers see [45-47].

2.5 Pre-filter synthesis

If the feedback system involves tracking signals, then the best choice is to use a pre-filter F. While controller G reduces the uncertainty and deals with stability, disturbance rejection, etc, pre-filter F is designed to fulfil tracking requirements [4].

2.6 Simulation and design validation

Once the controller design is finished, it is necessary to analyse the behaviour of the system with the controller previously obtained. Closed-loop response at several frequencies and time domain responses must be checked. The analysis will be carried out with the most unfavourable cases due to uncertainty [4].

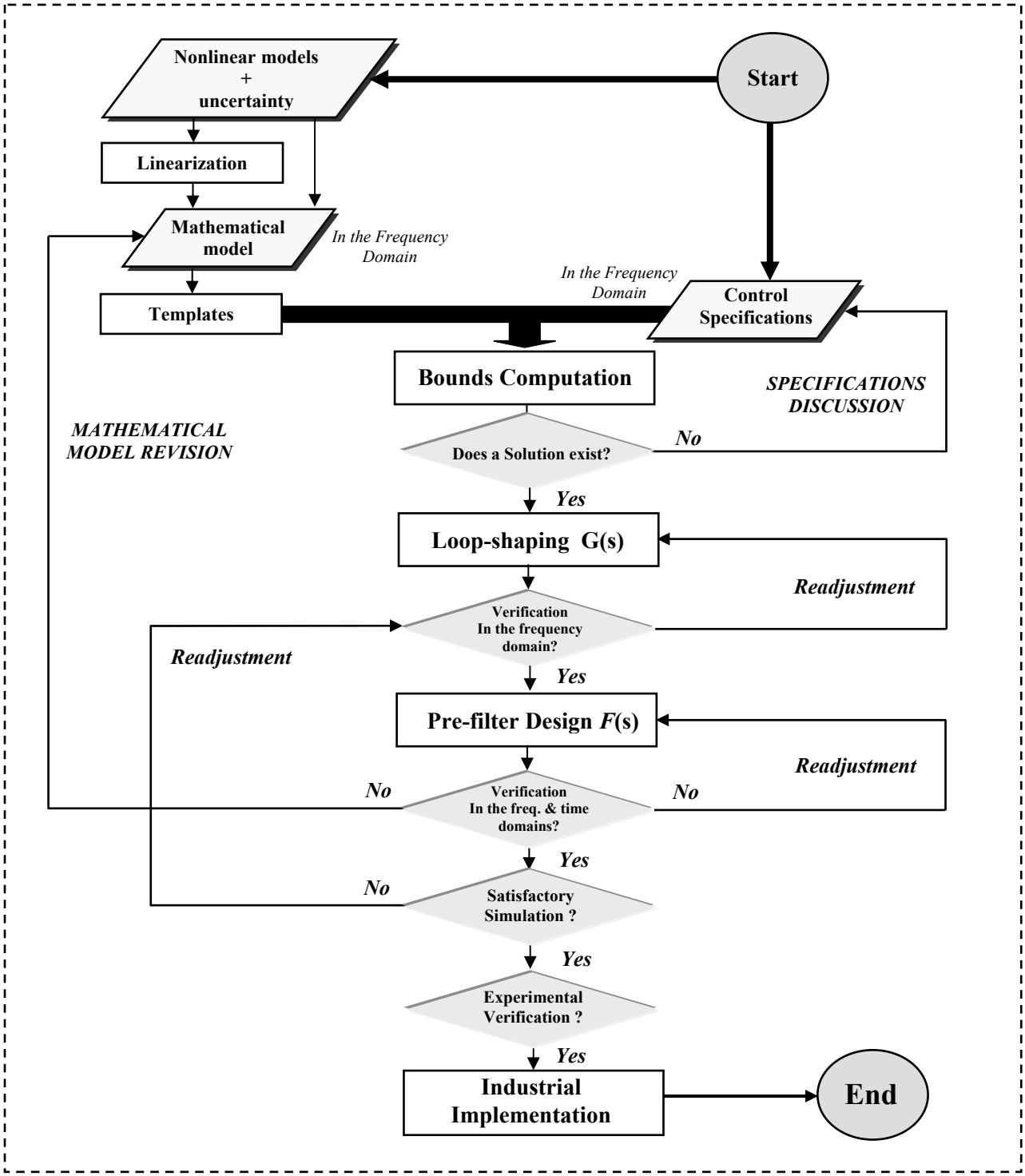

Figure 4: QFT methodology

3.0 QUANTITATIVE NON-DIAGONAL COMPENSATOR DESIGN FOR MIMO SYSTEMS [60],[62].

A fully populated matrix controller allows the designer much more design flexibility to govern MIMO processes than the classical diagonal controller structure. This section introduces a new methodology to extend the classical diagonal QFT controllers design for MIMO plants with model uncertainty to a fully populated matrix controller design. The section simultaneously studies three cases: the reference tracking, the external disturbance rejection at plant input and the external disturbance rejection at plant output. Therefore, the role played by the non-diagonal controller elements g_{ij} ($i \neq j$) is analysed in order to state a fully populated matrix controller design methodology for QFT. The definition of three coupling matrices (c_{1ij}, c_{2ij}, c_{3ij}) and a quality function q_{ij} of the non-diagonal elements come in useful to quantify the amount of loop interaction and to design the non-diagonal controllers respectively. This yields a criterion to propose a sequential design methodology of the fully populated matrix controller, in the QFT robust control frame. As a consequence the diagonal elements g_{kk} of the new non-diagonal method need less bandwidth than the diagonal elements of the previous diagonal methods. The work ends showing a real-world example (section 4), where an industrial SCARA robot manipulator is controlled using the new non-diagonal MIMO QFT methodology.

3.1 Introduction

Control of multivariable systems (multiple-input-multiple-output, MIMO) with model uncertainty are still one of the hardest problems that the control engineer has to face in real-world applications. Two of the main characteristics that define a MIMO system are the input and output directionality -different vectors to actuate U and to measure Y-; and the coupling among control loops -some outputs y_i can be influenced by several inputs u_i, and some inputs u_i can influence several outputs y_i.

In the last few decades a very significant amount of work in MIMO systems, too numerous to list, has been done. Useful techniques for designing multivariable feedback systems have been compiled in excellent references written by Rosenbrock [128], O'Reilly [129], Maciejowski [130], Skogestad and Postlethwaite [131], Houpis, Rasmussen and Garcia-Sanz [4], Marlin [132], Leithead and O'Reilly [133], etc. Some of them collect the frequency domain approach, firstly introduced and adopted by Rosenbrock and MacFarlane in the UK and by Horowitz in Israel, in the sixties, when most of the academic community regarded the frequency domain as obsolete for MIMO processes.

On the other hand, the original works in MIMO systems were only made for fixed plants, without any uncertainty in the model. The first technique that made a quantitative synthesis and took into account quantitative bounds on the plant uncertainty, and quantitative tolerances on the acceptable closed-loop system response, was introduced by Horowitz in the fifties [24] and subsequently reinforced and thoughtfully studied as it has been introduced in Section 2. That technique is the Quantitative Feedback Theory (QFT).

Using MIMO QFT, Horowitz [48-50] proposed to translate the original *nxn* MIMO problem into n^2 separate quantitative multiple-input-single-output MISO problems, each with plant uncertainty, external disturbances and closed-loop tolerances derived from the original problem.

The first improvement of the original MIMO QFT method was also introduced by Horowitz [52]. It obtains a significant reduction of over design in comparison with the previous method. It considers, in the successive steps of the iterative method, an equivalent plant that takes also into account the controllers designed in the previous steps. The book by Houpis, Rasmussen and Garcia-Sanz [4] presents a detailed compilation of both methods.

However, although such original MIMO QFT methods take the coupling among loops into account, they only propose the use of a diagonal controller $\boldsymbol{G}$ to govern the MIMO plant. This structure can be improved using non-diagonal controllers. In fact a fully populated matrix controller allows the designer much more design flexibility to control MIMO plants than the classical diagonal controller structure. The use of the non-diagonal components can also ease the diagonal controller design problem. The difficulty is how to design the off-diagonal elements, especially if one must consider engineering factors such as cost-benefit trade-offs of using cross-feeds, strong structure in the plant uncertainty, system integrity and plant input signal levels.

In the last few years some new methods for non-diagonal multivariable QFT robust control system design have been introduced. Again Horowitz designed and applied a procedure for non-diagonal $\boldsymbol{G}$ controllers [51]. The idea was to insert a non-diagonal matrix pre-compensator $\boldsymbol{H}$ before the plant, to have a new effective plant $\boldsymbol{P}_e = \boldsymbol{P}\,\boldsymbol{H}$. Later, Franchek and Nwokah presented a sequential loop frequency approach that utilizes a fully populated matrix controller to meet performance specifications, which may include system integrity requirements [56, 58]. Boje utilized the Perron-Frobenius root interaction measure to design a pre-compensator that reduces the level of coupling between loops, before a diagonal QFT controller matrix is attempted [59]. Yaniv introduced an approach that emphasizes the bandwidth of a non-diagonal pre-controller multiplied by the classical diagonal controller [57]. Kerr and Jayasuriya presented a non-sequential MIMO QFT methodology [63].

In this context, this section goes on with a previous work [60, 62] and introduces a new methodology, based on QFT, to extend the classical QFT diagonal controller design for MIMO plants with uncertainty to the fully populated matrix controller design. The work simultaneously studies three cases: the reference tracking, the external disturbance rejection at plant input and the external disturbance rejection at plant output. It presents the definition of three specific coupling matrices (c_{1ij}, c_{2ij}, c_{3ij}), one for each case. They come in useful to quantify the amount of the loop interaction of the system. Furthermore, a quality function q_{ij} of the non-diagonal elements g_{ij} ($i \neq j$) for the three problems is utilized to aid the design of the fully populated matrix controllers. Based on the above ideas, the work introduces a sequential design methodology for non-diagonal QFT controllers. It contemplates the design of quantitative controllers able to achieve reference tracking and disturbance rejection specifications, taking also into account the reduction of interaction among loops. The diagonal elements g_{kk} of the new non-diagonal method need less bandwidth than the diagonal elements of the previous diagonal methods.

The work begins with two sub-sections that formulate the coupling matrices and the coupling elements of the control system. Then the fourth sub-section introduces the expressions of the optimum non-diagonal controller. Sub-section five analyses and compares the coupling effects among loops of both, the classical diagonal method and the new non-diagonal methodology. Sub-section six introduces a quality function to quantify the amount of loop interaction and to design the non-diagonal controllers. Sub-section seven presents the sequential procedure to design the fully populated matrix controller. Sub-section eight deals with some practical issues for using the method. Section 4 applies the new MIMO QFT methodology to control a real-world problem: a SCARA robot manipulator [115].

3.2 The Coupling Matrix

The objective of this section is to define a measurement index (the coupling matrix) that allows one to quantify the loop interaction in MIMO control systems. Consider a nxn linear multivariable system -see Fig. 5-, composed of a plant $\boldsymbol{P}$, a fully populated matrix controller $\boldsymbol{G}$, a pre-filter $\boldsymbol{F}$, a plant input disturbance transfer function $\boldsymbol{P}_{di}$, and a plant output disturbance transfer function $\boldsymbol{P}_{do}$, where $\boldsymbol{P} \in \Im\mathbf{P}$, $\Im\mathbf{P}$ is the set of possible plants due to uncertainty, and,

$$\boldsymbol{P}=\begin{bmatrix} p_{11} & p_{12} & \cdots & p_{1n} \\ p_{21} & p_{22} & \cdots & p_{2n} \\ \cdots & \cdots & \cdots & \cdots \\ p_{n1} & p_{n2} & \cdots & p_{nn} \end{bmatrix};\ \boldsymbol{G}=\begin{bmatrix} g_{11} & g_{12} & \cdots & g_{1n} \\ g_{21} & g_{22} & \cdots & g_{2n} \\ \cdots & \cdots & \cdots & \cdots \\ g_{n1} & g_{n2} & \cdots & g_{nn} \end{bmatrix};\ \boldsymbol{F}=\begin{bmatrix} f_{11} & f_{12} & \cdots & f_{1n} \\ f_{21} & f_{22} & \cdots & f_{2n} \\ \cdots & \cdots & \cdots & \cdots \\ f_{n1} & f_{n2} & \cdots & f_{nn} \end{bmatrix} \tag{17}$$

The reference vector $\boldsymbol{r}'$ and the external disturbance vectors at plant input $\boldsymbol{d}_i'$ and plant output $\boldsymbol{d}_o'$ are the inputs of the system. The output vector y is the variable to be controlled.

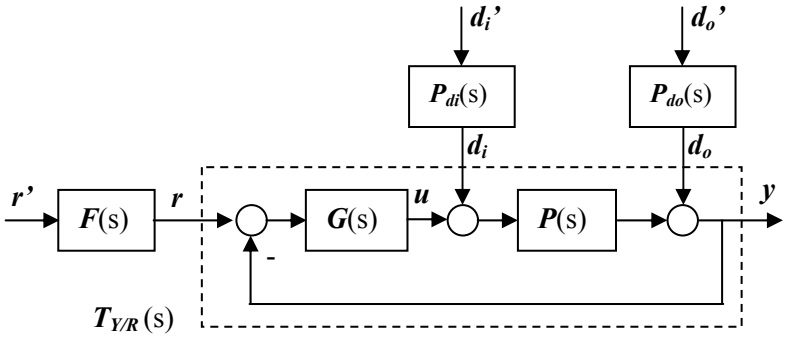

Fig. 5 Structure of a 2 Degree of Freedom MIMO System

It is denoted $\boldsymbol{P}^*$ as the plant inverse so that,

$$\boldsymbol{P}^{-1}=\boldsymbol{P}^*=\left[p_{ij}^*\right]=\boldsymbol{\Lambda}+\boldsymbol{B}=\begin{bmatrix} p_{11}^* & 0 & 0 \\ 0 & \cdots & 0 \\ 0 & 0 & p_{nn}^* \end{bmatrix}+\begin{bmatrix} 0 & \cdots & p_{1n}^* \\ \cdots & 0 & \cdots \\ p_{n1}^* & \cdots & 0 \end{bmatrix} \tag{18}$$

$$\boldsymbol{G}=\boldsymbol{G}_{\boldsymbol{d}}+\boldsymbol{G}_{\boldsymbol{b}}=\begin{bmatrix} g_{11} & 0 & 0 \\ 0 & \cdots & 0 \\ 0 & 0 & g_{nn} \end{bmatrix}+\begin{bmatrix} 0 & \cdots & g_{1n} \\ \cdots & 0 & \cdots \\ g_{n1} & \cdots & 0 \end{bmatrix} \tag{19}$$

where $\boldsymbol{\Lambda}$ is the diagonal part and $\boldsymbol{B}$ is the balance of $\boldsymbol{P}^*$; and $\boldsymbol{G}_{\mathrm{d}}$ is the diagonal part and $\boldsymbol{G}_{\mathrm{b}}$ is the balance of $\boldsymbol{G}$.

The next paragraphs introduce a measurement index to quantify the loop interaction in the three classical cases: reference tracking, external disturbances at plant input, and external disturbances at plant output. That index is called the *coupling matrix* and, depending on the case, shows three different expressions: $\boldsymbol{C}_1$, $\boldsymbol{C}_2$, $\boldsymbol{C}_3$ respectively.

3.2.1 Tracking

The transfer function matrix of the controlled system for the reference tracking problem, without any external disturbance, can be written as shown in Eq. (20),

$$\boldsymbol{y}=(\boldsymbol{I}+\boldsymbol{P}\,\boldsymbol{G})^{-1}\,\boldsymbol{P}\,\boldsymbol{G}\,\boldsymbol{r}=\boldsymbol{T}_{\boldsymbol{y}/\boldsymbol{r}}\,\boldsymbol{r}=\boldsymbol{T}_{\boldsymbol{y}/\boldsymbol{r}}\,\boldsymbol{F}\,\boldsymbol{r}' \tag{20}$$

Using Eq. (18) and (19), Eq. (20) can be rewritten as,

$$\boldsymbol{T}_{y/r}\ \boldsymbol{r} = \left(\boldsymbol{I} + \boldsymbol{\Lambda}^{-1}\ \boldsymbol{G}_{\mathrm{d}}\right)^{-1}\ \boldsymbol{\Lambda}^{-1}\ \boldsymbol{G}_{\mathrm{d}}\ \boldsymbol{r} + \left(\boldsymbol{I} + \boldsymbol{\Lambda}^{-1}\ \boldsymbol{G}_{\mathrm{d}}\right)^{-1}\ \boldsymbol{\Lambda}^{-1}\left(\boldsymbol{G}_{\mathrm{b}}\ \boldsymbol{r} - (\boldsymbol{B} + \boldsymbol{G}_{\mathrm{b}})\ \boldsymbol{T}_{y/r}\ \boldsymbol{r}\right) \qquad \textbf{(21)}$$

In the expression of the closed-loop transfer function matrix of Eq. (21), it is possible to find two different terms:

i. A diagonal term $\boldsymbol{T}_{\mathrm{y/r\_d}}$,

$$\boldsymbol{T}_{\mathrm{y/r\_d}} = \left(\boldsymbol{I} + \boldsymbol{\Lambda}^{-1}\ \boldsymbol{G}_{\mathrm{d}}\right)^{-1}\ \boldsymbol{\Lambda}^{-1}\ \boldsymbol{G}_{\mathrm{d}} \qquad \textbf{(22)}$$

that presents a diagonal structure. Note that it does not depend on the non-diagonal part of the plant inverse $\boldsymbol{B}$ nor on the non-diagonal part of the controller $\boldsymbol{G}_{\mathrm{b}}$. It is equivalent to n reference tracking SISO systems formed by plants equal to the elements of $\boldsymbol{\Lambda}^{-1}$ when the n corresponding parts of a diagonal $\boldsymbol{G}_{\mathrm{d}}$ control them, as shown in Fig. 6a.

ii. A non-diagonal term $\boldsymbol{T}_{\mathrm{y/r\_b}}$,

$$\boldsymbol{T}_{\mathrm{y/r\_b}} = \left(\boldsymbol{I} + \boldsymbol{\Lambda}^{-1}\ \boldsymbol{G}_{\mathrm{d}}\right)^{-1}\ \boldsymbol{\Lambda}^{-1}\left[\boldsymbol{G}_{\mathrm{b}} - (\boldsymbol{B} + \boldsymbol{G}_{\mathrm{b}})\ \boldsymbol{T}_{y/r}\right] = \left(\boldsymbol{I} + \boldsymbol{\Lambda}^{-1}\ \boldsymbol{G}_{\mathrm{d}}\right)^{-1}\ \boldsymbol{\Lambda}^{-1}\ \boldsymbol{C}_{1} \qquad \textbf{(23)}$$

that presents a non-diagonal structure. It is equivalent to the same n previous systems with internal disturbances $c_{1\mathrm{ij}}\ r_{\mathrm{j}}$ at plant input (Fig. 6b).

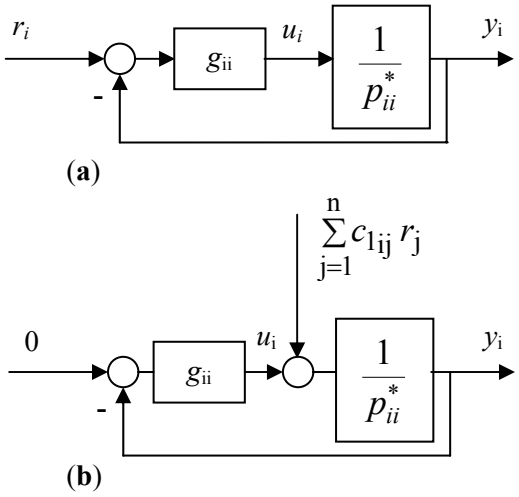

Fig. 6 i-th equivalent SISO and MISO systems

In Eq. (23), the matrix $\boldsymbol{C}_1$ is the only part that depends on the non-diagonal parts of both the plant inverse $\boldsymbol{B}$ and the controller $\boldsymbol{G}_{\mathrm{b}}$. Hence, it comprises the coupling, and from now on $\boldsymbol{C}_1$ will be the *coupling matrix* of the equivalent system for reference tracking problems,

$$\boldsymbol{C}_1 = \boldsymbol{G}_{\boldsymbol{b}} - (\boldsymbol{B} + \boldsymbol{G}_{\boldsymbol{b}})\ \boldsymbol{T}_{y/r} \qquad \textbf{(24)}$$

Each element c_{1ij} of this matrix obeys,

$$c_{1ij} = g_{ij}\,(1-\delta_{ij}) - \sum_{k=1}^{n} (p^{*}_{ik} + g_{ik})\, t_{kj}\,(1-\delta_{ik}) \tag{25}$$

where δ_{ki} is the delta of Kronecker that is defined as,

$$\delta_{ki} = \begin{cases} \delta_{ki} = 1 \Leftrightarrow k = i \\ \delta_{ki} = 0 \Leftrightarrow k \neq i \end{cases} \tag{26}$$

3.2.2 Disturbance rejection at plant input

The transfer matrix from the external disturbance at plant input $\boldsymbol{d_i'}$ to the output y can be written as shown in Eq. (27),

$$\boldsymbol{y} = (\boldsymbol{I} + \boldsymbol{P}\,\boldsymbol{G})^{-1}\,\boldsymbol{P}\,\boldsymbol{d_i} = \boldsymbol{T_{y/di}}\,\boldsymbol{d_i} = \boldsymbol{T_{y/di}}\,\boldsymbol{P_{di}}\,\boldsymbol{d_i'} \tag{27}$$

and then,

$$\boldsymbol{T}_{y/di}\,\boldsymbol{d}_i = \left(\boldsymbol{I} + \boldsymbol{\Lambda}^{-1}\,\boldsymbol{G}_d\right)^{-1}\,\boldsymbol{\Lambda}^{-1}\,\boldsymbol{d}_i - \left(\boldsymbol{I} + \boldsymbol{\Lambda}^{-1}\,\boldsymbol{G}_d\right)^{-1}\,\boldsymbol{\Lambda}^{-1}\left(\left(\boldsymbol{B} + \boldsymbol{G}_b\right)\boldsymbol{T}_{y/di}\right)\boldsymbol{d}_i \tag{28}$$

In that expression -Eq. (28)- it is possible to find two different terms:

i. A diagonal term $\boldsymbol{T}_{y/di\_d}$,

$$\boldsymbol{T}_{y/di\_d} = \left(\boldsymbol{I} + \boldsymbol{\Lambda}^{-1}\,\boldsymbol{G}_d\right)^{-1}\,\boldsymbol{\Lambda}^{-1} \tag{29}$$

Again, Eq. (29) is equivalent to n regulator MISO systems, as shown in Fig. 7a.

ii. Non diagonal term $\boldsymbol{T}_{y/di\_b}$

$$\boldsymbol{T}_{y/di\_b} = \left(\boldsymbol{I} + \boldsymbol{\Lambda}^{-1}\,\boldsymbol{G}_d\right)^{-1}\,\boldsymbol{\Lambda}^{-1}\left(\boldsymbol{B} + \boldsymbol{G}_b\right)\boldsymbol{T}_{y/di} = \left(\boldsymbol{I} + \boldsymbol{\Lambda}^{-1}\,\boldsymbol{G}_d\right)^{-1}\,\boldsymbol{\Lambda}^{-1}\,\boldsymbol{C}_2 \tag{30}$$

that presents a non-diagonal structure which is equivalent to the same n previous systems with external disturbances $c_{2ij}\,di_j$ at plant input, as shown in Fig. 7b.

In Eq. (30), the matrix $\boldsymbol{C}_2$ comprises the coupling, and from now on $\boldsymbol{C}_2$ will be the *coupling matrix* of the equivalent system for external disturbance rejection at plant input problems,

$$\boldsymbol{C}_2 = (\boldsymbol{B} + \boldsymbol{G_b})\,\boldsymbol{T}_{y/di} \tag{31}$$

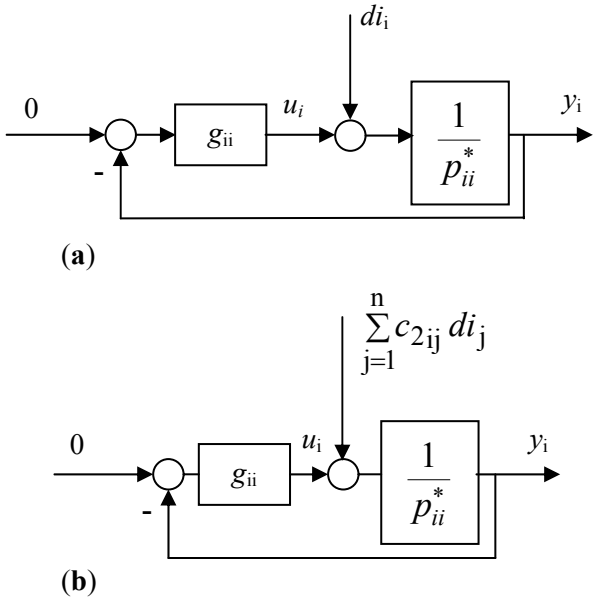

Fig. 7 i-th equivalent MISO systems

Each element c_{2ij} of this matrix obeys,

$$c_{2ij} = \sum_{k=1}^{n} (p^*_{ik} + g_{ik})\, t_{kj}\, (1 - \delta_{ik}) \tag{32}$$

where δ_{ki} is the delta of Kronecker defined in Equation (26).

3.2.3 Disturbance rejection at plant output

The transfer matrix from the external disturbance at plant output $\boldsymbol{d}'_{\boldsymbol{o}}$ to the output y can be written as shown in Eq. (33),

$$\boldsymbol{y} = (\boldsymbol{I} + \boldsymbol{P}\,\boldsymbol{G})^{-1}\, \boldsymbol{d}_{\boldsymbol{o}} = \boldsymbol{T}_{\boldsymbol{y}/\boldsymbol{do}}\, \boldsymbol{d}_{\boldsymbol{o}} = \boldsymbol{T}_{\boldsymbol{y}/\boldsymbol{do}}\, \boldsymbol{P}_{\boldsymbol{do}}\, \boldsymbol{d}'_{\boldsymbol{o}} \tag{33}$$

and then,

$$\boldsymbol{T}_{\boldsymbol{y}/\boldsymbol{do}}\, \boldsymbol{d}_{\boldsymbol{o}} = \left(\boldsymbol{I} + \boldsymbol{\Lambda}^{-1}\, \boldsymbol{G}_{\mathrm{d}}\right)^{-1}\, \boldsymbol{d}_{\boldsymbol{o}} + \left(\boldsymbol{I} + \boldsymbol{\Lambda}^{-1}\, \boldsymbol{G}_{\mathrm{d}}\right)^{-1}\, \boldsymbol{\Lambda}^{-1}\, \left(\boldsymbol{B} - (\boldsymbol{B} + \boldsymbol{G}_{\mathrm{b}})\, \boldsymbol{T}_{\boldsymbol{y}/\boldsymbol{do}}\right) \boldsymbol{d}_{\boldsymbol{o}} \tag{34}$$

In that expression -Eq. (34)- it is possible to find two different terms:

i. A diagonal term $\boldsymbol{T}_{\mathrm{y/do\_d}}$,

$$\boldsymbol{T}_{\mathrm{y/do\_d}} = \left(\boldsymbol{I} + \boldsymbol{\Lambda}^{-1}\, \boldsymbol{G}_{\mathrm{d}}\right)^{-1} \tag{35}$$

Once more, Eq. (35) is equivalent to the n regulator MISO systems showed in Fig. 8a,

ii. Non diagonal term $\boldsymbol{T}_{\text{y/do\_b}}$

$$\boldsymbol{T}_{\text{y/do\_b}} = \left(\boldsymbol{I} + \boldsymbol{\Lambda}^{-1}\ \boldsymbol{G}_{\text{d}}\right)^{-1}\ \boldsymbol{\Lambda}^{-1}\left[\boldsymbol{B} - \left(\boldsymbol{B} + \boldsymbol{G}_{\text{b}}\right)\boldsymbol{T}_{\boldsymbol{y/do}}\right] = \left(\boldsymbol{I} + \boldsymbol{\Lambda}^{-1}\ \boldsymbol{G}_{\text{d}}\right)^{-1}\ \boldsymbol{\Lambda}^{-1}\ \boldsymbol{C}_3 \tag{36}$$

that presents a non-diagonal structure. It is equivalent to the same n previous systems with external disturbances $c_{3\text{ij}}\ do_{\text{j}}$ at plant input, as shown Fig. 8b.

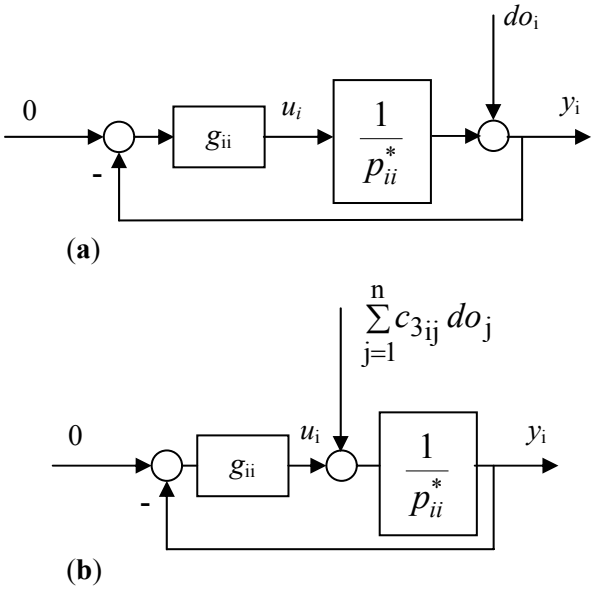

Fig. 8 i-th equivalent MISO systems

In Eq. (36), the matrix $\boldsymbol{C}_3$ comprises the coupling, and from now on it will be the *coupling matrix* of the equivalent system for external disturbance rejection at plant output problems,

$$\boldsymbol{C}_3 = \boldsymbol{B} - \left(\boldsymbol{B} + \boldsymbol{G}_b\right)\boldsymbol{T}_{\boldsymbol{y/do}} \tag{37}$$

Each element of the coupling matrix, $c_{3\text{ij}}$ obeys,

$$c_{3\text{ij}} = p^*_{\text{ij}}\ (1 - \delta_{\text{ij}}) - \sum_{k=1}^{\text{n}} (p^*_{\text{ik}} + g_{\text{ik}})\ t_{\text{kj}}\ (1 - \delta_{\text{ik}}) \tag{38}$$

where δ_{ki} is the delta of Kronecker as defined in Equation (26).

3.3 The Coupling Elements

In order to design a MIMO controller with a low coupling level, it is necessary to study the influence of every non-diagonal element g_{ij} on the coupling elements $c_{1\text{ij}}$, $c_{2\text{ij}}$ and $c_{3\text{ij}}$, defined in Eq. (25), (32) and (38).

These elements can be simplified to quantify the coupling effects. Then it will be possible to analyse the loop decoupling and to state some conditions and limitations using fully populated matrix controllers.

To analyse the coupling elements, one Hypothesis is stated.

Hypothesis H1: suppose that in Eq. (25), (32) and (38),

$$\left|\left(p_{ij}^{*}+g_{ij}\right)t_{jj}\right| >> \left|\left(p_{ik}^{*}+g_{ik}\right)t_{kj}\right|, \text{ for } k \neq j, \text{ and in the bandwidth of } t_{jj} \quad \textbf{(39)}$$

Note that the above expression is scale invariant and is typically fulfilled once the MIMO system has been ordered according to appropriate methods like the Relative Gain Analysis [134], etc. Then the diagonal elements t_{jj} will be much larger that the non-diagonal ones t_{kj},

$$\left|t_{jj}\right| >> \left|t_{kj}\right|, \text{ for } k \neq j, \text{ and in the bandwidth of } t_{jj} \quad \textbf{(40)}$$

Now, two simplifications are applied to facilitate the quantification of the coupling effects c_{1ij}, c_{2ij}, c_{3ij}.

Simplification S1: Using the Hypothesis H1, Eqs. (25), (32) and (38), which describe the coupling elements in the tracking problem, disturbance rejection at plant input and disturbance rejection at plant output respectively, are rewritten as shown Table III.

Simplification S2: The elements t_{jj} are computed for each case from the equivalent system derived from Eqs. (22), (29) and (35). The results are shown in Table III.

Table III: Simplifications to quantify the coupling effects

	Reference tracking	**External disturbances at plant input**	**External disturbances at plant output**
Simplification S1	$c_{1ij} = g_{ij} - t_{jj}\left(p_{ij}^{*}+g_{ij}\right)$; $i \neq j$ **(41)**	$c_{2ij} = t_{jj}\left(p_{ij}^{*}+g_{ij}\right)$; $i \neq j$ **(42)**	$c_{3ij} = p_{ij}^{*} - t_{jj}\left(p_{ij}^{*}+g_{ij}\right)$; $i \neq j$ **(43)**
Simplification S2	$t_{jj} = \dfrac{g_{jj}\ p_{jj}^{*-1}}{1+g_{jj}\ p_{jj}^{*-1}}$ **(44)**	$t_{jj} = \dfrac{p_{jj}^{*-1}}{1+g_{jj}\ p_{jj}^{*-1}}$ **(45)**	$t_{jj} = \dfrac{1}{1+g_{jj}\ p_{jj}^{*-1}}$ **(46)**

Due to Simplifications S1 and S2, the coupling effects c_{1ij}, c_{2ij}, c_{3ij} can be computed as,

Tracking

$$c_{1ij} = g_{ij} - \frac{g_{jj}\left(p_{ij}^{*}+g_{ij}\right)}{\left(p_{jj}^{*}+g_{jj}\right)} \quad ; \quad i \neq j \quad \textbf{(47)}$$

Disturbance rejection at plant input

$$c_{2ij} = \frac{\left(p_{ij}^{*}+g_{ij}\right)}{\left(p_{jj}^{*}+g_{jj}\right)} \quad ; \quad i \neq j \quad \textbf{(48)}$$

Disturbance rejection at plant output

$$c_{3ij} = p^*_{ij} - \frac{p^*_{jj}\left(p^*_{ij} + g_{ij}\right)}{\left(p^*_{jj} + g_{jj}\right)} \quad ; \quad i \neq j \tag{49}$$

3.4 The Optimum Non-diagonal Controller

Consider non-diagonal controllers to reduce the coupling effect, as well as diagonal controllers that help to achieve the loop performance specifications. The optimum non-diagonal controllers for the three cases (tracking and disturbance rejection at plant input and output) can be obtained making the loop interaction of Eqs. (47), (48) and (49) equal to zero.

Note that both elements, p^*_{ij} and p^*_{jj}, of these equations are uncertain elements of $\boldsymbol{P}^*$. Every uncertain plant p^*_{ij} can be any plant represented by the family,

$$\left\{p^*_{ij}\right\} = p^{*N}_{ij}\left(1 + \Delta_{ij}\right) \ , \ 0 \le \left|\Delta_{ij}\right| \le \Delta\, p^*_{ij} \ , \ \text{for } i, j = 1,...,n \tag{50}$$

where p^{*N}_{ij} is the nominal plant, and Δp^*_{ij} the maximum of the non-parametric uncertainty radii $\left|\Delta_{ij}\right|$.

The nominal plants p^{*N}_{ij} and p^{*N}_{jj} that will be chosen for the optimum non-diagonal controller will follow the next rules:

a) If the uncertain parameters of the plants show a uniform Probability Distribution (Fig. 9a) –which is typical in the QFT methodology-, then the elements p^*_{ij} and p^*_{jj} for the optimum non-diagonal controller will be the nominal plants p^{*N}_{ij} and p^{*N}_{jj}, which minimise the maximum of the non-parametric uncertainty radii Δp^*_{ij} and Δp^*_{jj} that comprise the plant templates (Fig. 9b).

b) If the uncertain parameters of the plants show a non-uniform Probability Distribution (Fig. 9c), then the elements p^*_{ij} and p^*_{jj} for the optimum non-diagonal controller will be the nominal plants p^{*N}_{ij} and p^{*N}_{jj}, whose set of parameters maximize the area of the Probability Distribution in the regions $[\, a_{ij} - \varepsilon, a_{ij} + \varepsilon \,]$ and $[\, a_{jj} - \varepsilon, a_{jj} + \varepsilon \,]$ ($\forall$ parameter a_{ij}, b_{ij}, …, a_{jj}, b_{jj} …) respectively.

These rules of selection will be analysed again in Section 4.5, when we compute the coupling effects with the optimum non-diagonal controller.

Now, making Eqs. (47), (48) and (49) equal to zero and using Eq. (50), the optimum non-diagonal controller for each case is obtained.

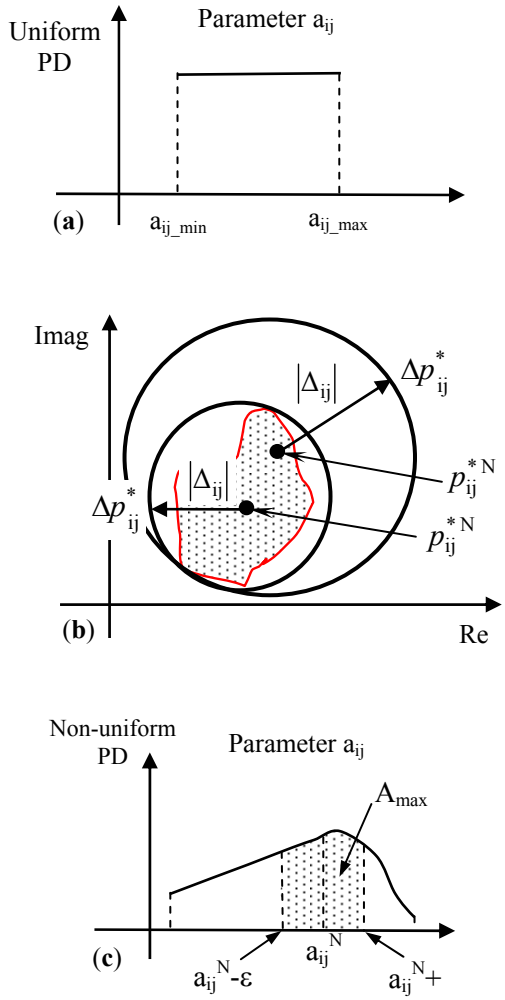

Fig. 9 Probability Distribution of the parameter a_{ij}, and Non-parametric uncertainty radii Δp^*_{ij} that comprise the plant templates

3.4.1 Tracking

$$g_{ij}^{opt} = F_{pd}\left(g_{jj} \frac{p_{ij}^{*N}}{p_{jj}^{*N}} \right), \text{ for } i \neq j \qquad \textbf{(51)}$$

3.4.2 Disturbance rejection at plant input

$$g_{ij}^{opt} = F_{pd}\left(-p_{ij}^{*N} \right), \text{ for } i \neq j \qquad \textbf{(52)}$$

3.4.3 Disturbance rejection at plant output

$$g_{ij}^{opt} = F_{pd}\left(g_{jj} \frac{p_{ij}^{*N}}{p_{jj}^{*N}} \right), \text{ for } i \neq j \qquad \textbf{(53)}$$

where the function $F_{pd}(A)$ means in every case a proper function made from the dominant poles and zeros of the expression A.

3.5 The Coupling Effects

The minimum achievable coupling effects -Eqs. (54), (56), (58)- can be computed substituting the optimum controller of Eqs. (51), (52) and (53) in the coupling expressions of Eqs. (47), (48) and (49) respectively, and taking into account the uncertainty radii of Eq. (50). Analogously, the maximum coupling effect without any non-diagonal controller -pure diagonal controller cases- can be computed substituting g_{ij}=0 in the Eqs. (47), (48) and (49) respectively -Eqs. (55), (57), (59)-. That is to say,

3.5.1 Tracking

$$\left| c_{1ij} \right|_{g_{ij}=g_{ij}^{opt}} = \left| \psi_{ij} \left(\Delta_{jj} - \Delta_{ij} \right) g_{jj} \right| \qquad \textbf{(54)}$$

$$\left| c_{1ij} \right|_{g_{ij}=0} = \left| \psi_{ij} \left(1 + \Delta_{ij} \right) g_{jj} \right| \qquad \textbf{(55)}$$

3.5.2 Disturbance rejection at plant input

$$\left| c_{2ij} \right|_{g_{ij}=g_{ij}^{opt}} = \left| \psi_{ij} \, \Delta_{ij} \right| \qquad \textbf{(56)}$$

$$\left| c_{2ij} \right|_{g_{ij}=0} = \left| \psi_{ij} \left(1 + \Delta_{ij} \right) \right| \qquad \textbf{(57)}$$

3.5.3 Disturbance rejection at plant output

$$\left| c_{3ij} \right|_{g_{ij}=g_{ij}^{opt}} = \left| \psi_{ij} \left(\Delta_{ij} - \Delta_{jj} \right) g_{jj} \right| \qquad \textbf{(58)}$$

$$\left| c_{3ij} \right|_{g_{ij}=0} = \left| \psi_{ij} \left(1 + \Delta_{ij} \right) g_{jj} \right| \qquad \textbf{(59)}$$

where,

$$\psi_{ij} = \frac{p_{ij}^{*N}}{\left(1 + \Delta_{jj} \right) p_{jj}^{*N} + g_{jj}} \qquad \textbf{(60)}$$

and the uncertainty is: $0 \le \left| \Delta_{ij} \right| \le \Delta p_{ij}^{*}$, $0 \le \left| \Delta_{jj} \right| \le \Delta p_{jj}^{*}$, for $i, j = 1, \ldots, n$

The coupling effects, calculated in the pure diagonal controller cases, result in three expressions (55), (57) and (59) that still present a non-zero value when the nominal-actual plant mismatching due to the uncertainty disappears: $\Delta_{ij} = 0$ and $\Delta_{jj} = 0$. However, the coupling effects obtained with the optimum non-diagonal controllers -Eqs. (54), (56) and (58)- tends to zero when that mismatching disappears.

3.6 Quality of the Designed Controller

Fig. 10 shows the appearance of three different coupling bands for a common process. The maximum $|c_{ij}|_{gij=0}$ -computed from Eqs. (55), (57) or (59)- and the minimum coupling effects without any non-diagonal controller g_{ij} limit the first one, as well as the second one is bounded by the maximum and the minimum coupling effects with a non-optimum decoupling element g_{ij}. Finally, the minimum coupling effect $|c_{ij}|_{gij=gij}^{opt}$ with the optimum decoupling element g_{ij}^{opt} presents a maximum value, computed from Eqs. (54), (56) or (58).

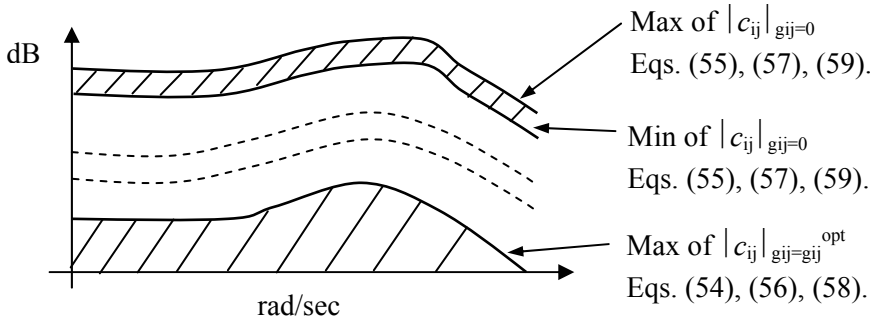

Fig. 10 Coupling effect bands with different non-diagonal controllers

From those ideas a quality function q_{ij} is defined for a non-diagonal controller g_{ij} (i≠j) so that,

$$q_{ij}(\%) = 100 \left\{ \frac{\log_{10}\left[\dfrac{\max\{|c_{ij}|_{g_{ij}=0}\}}{\max\{|c_{ij}|_{g_{ij}=g_{ij}}\}} \right]}{\log_{10}\left[\dfrac{\max\{|c_{ij}|_{g_{ij}=0}\}}{\max\{|c_{ij}|_{g_{ij}=g_{ij}^{opt}}\}} \right]} \right\} \qquad \textbf{(61)}$$

The quality function becomes a proximity measure of the coupling effect c_{ij} to the minimum achievable coupling effect. Thus, the quality function is useful to quantify the amount of loop interaction and to design the non-diagonal controllers. A suitable non-diagonal controller will maximise the quality function of Eq. (61).

3.7 Design Methodology

The proposed controller design method is a sequential procedure closing loops [58]. It uses a fully populated matrix controller that does not assign any special role to the upper and lower triangular elements of the controller ***G***, and in addition, it can be used to design the feedback controller of a 2DOF structure (see Fig. 5). First it is necessary to fulfil the Hypothesis H1 and two new Hypotheses H2 and H3.

Hypothesis H2: The plant $\boldsymbol{P}$ and its inverse $\boldsymbol{P}^*$ have to be stable and do not have any hidden unstable mode. Despite looking very restrictive, note that it is only a sufficient condition to guarantee the stability of the system. Consequently, the designer must pay close attention to systems with non-minimum phase or unstable elements [58, 61].

In the last few years, several works have studied the stability problem of MIMO systems with uncertainty, using inverse plants in the QFT methodology. A deep analysis of the subject can be found in the next four references: [61, 106, 4, 5]. The second paper proofs that it is necessary and sufficient that the plant of each successive loop is stabilised. The third and fourth references expand the analysis.

Hypothesis H3: The plant $\boldsymbol{P}$ is not 'ill-conditioned' for any of the possible plants in the whole set $\Im\mathbf{P}$. This will guarantee the robustness of the design. It is known [135] that 'ill-conditioned' plants, with large elements of the RGA -Relative Gain Analysis [134]- matrix are difficult to control.

Methodology

Step A. First, the methodology begins paring inputs and outputs with the RGA technique [134], and arranging the matrix $\boldsymbol{P}^*$ so that $\left(p_{11}^*\right)^{-1}$ has the smallest phase margin frequency, $\left(p_{22}^*\right)^{-1}$ the next smallest phase margin frequency, and so on [4]. Later, the sequential controller design technique (Fig. 11), composed of n stages -n loops-, will follow the next steps (B and C) for every column k = 1 to n.

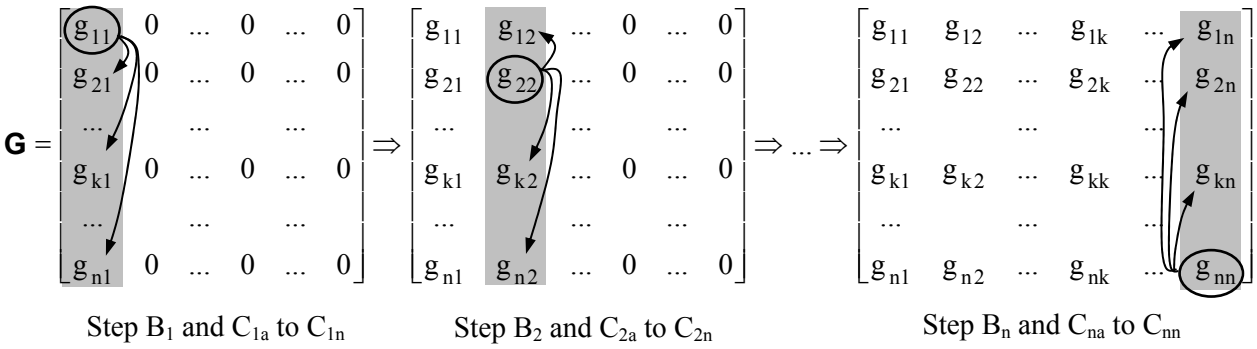

Fig. 11 Steps for controllers design

Step B. Design the diagonal controller g_{kk}. This design stage of g_{kk} is calculated through standard QFT loop-shaping for the inverse of the equivalent plant $\left(p_{kk}^{*e}\right)^{-1}$ in order to achieve robust stability and robust performance specifications. The equivalent plant satisfies the next recursive relationship [58],

$$\left[p_{ii}^{*e}\right]_k = \left[p_{ii}^*\right]_{k-1} - \frac{\left(\left[p_{i(i-1)}^*\right]_{k-1} + \left[g_{i(i-1)}\right]_{k-1}\right)\left(\left[p_{(i-1)i}^*\right]_{k-1} + \left[g_{(i-1)i}\right]_{k-1}\right)}{\left[p_{(i-1)(i-1)}^*\right]_{k-1} + \left[g_{(i-1)(i-1)}\right]_{k-1}};\ i \geq k;\quad \left[\boldsymbol{P}^*\right]_{k=1} = \boldsymbol{P}^* \qquad \textbf{(62)}$$

which is an extension for the non-diagonal case of the recursive expression proposed by Horowitz [52] as the *Improved design technique*, also called *Second method* by Houpis *et al.* [4].

If the control system requires tracking specifications as $a_{ii}(\omega) \leq \left|t_{ii}^{y/r}(j\omega)\right| \leq b_{ii}(\omega)$ then, because $t_{ii}^{y/r} = t_{rii} + t_{c1ii}$ -Eq.(21)-, the tracking bounds b_{ii} and a_{ii} will have to be corrected with the coupling

specification τ_{c1ii}, so that:

$$b_{ii}^{c} = b_{ii} - \tau_{c1ii} \quad , \quad a_{ii}^{c} = a_{ii} + \tau_{c1ii} \tag{63}$$

$$t_{c1ii} = w_{ii}\ c_{1ii} \le \tau_{c1ii} \tag{64}$$

$$a_{ii}^{c}(\omega) \le |t_{rii}(j\omega)| \le b_{ii}^{c}(\omega) \tag{65}$$

These are the same corrections proposed by Horowitz [48, 52] and Houpis, Rasmussen and Garcia-Sanz [4] for the original MIMO QFT methods 1 and 2.

However, with the new non-diagonal method these corrections will be less demanding. The coupling expression $t_{c1ii} = w_{ii}\ c_{1ii}$ is now minor than in the previous diagonal methods –compare Eqs. (54) and (55)-. The off-diagonal elements g_{ij} (i≠j) of the matrix controller will attenuate or cancel that cross coupling. Then the diagonal elements g_{kk} of the non-diagonal method will need less bandwidth than the diagonal elements of the previous diagonal methods.

Step C. Design the (n-1) non-diagonal elements g_{ik} (i ≠ k, i = 1,2,...n) of the k-th controller column, minimising the coupling c_{ik} -computed from Eqs. (47), (48) and (49)-. To achieve this goal, the nominal optimum controller -Eqs. (51), (52) and (53)- must be taken into account.

Step D. Finally, the design of the pre-filter ***F*** does not present any difficulty, if the complementary sensitivity function shows a low level of loop interaction. Therefore, the pre-filter ***F*** can be diagonal.

3.8 Some Practical Issues

To use the above controllers there is a relevant condition to take into account: the plant ***P*** and its inverse $\boldsymbol{P}^{*}$ have to be stable and do not have any hidden unstable mode –The H2 Hypothesis- [58]. This is only a sufficient condition. Hence, in some cases of not fulfilling this condition it is even possible to use a non-diagonal controller element like the above-mentioned [63]. In these situations some difficulties might appear during the sequential procedure such as the introduction of additional non-minimum phase (nmp) zeros due to hidden unstable modes of the plant or due to loop closures. This typically occurs in highly coupled systems.

To avoid this problem, the elements of the resulting plants $\left(p_{kk}^{*e}\right)^{-1}$ must be checked in every step of the design methodology to ensure that right half plane transmission zeros or unstable modes have not been introduced by the new controller elements g_{kk} or g_{ik}, which would obviously cause an unnecessary loss of control performance [58]. If these nmp zeros appear due to the designed controller elements, supplementary constraints in the determinant of ***PG*** should be imposed to re-calculate the controller. On the other hand, if the plant elements, p_{kk} or p_{ik}, are the cause of the introduction of non-minimum phase elements in the equivalent plant $\left(p_{kk}^{*e}\right)^{-1}$, the theory proposed for nmp MISO feedback systems by Horowitz *et al.* [3, 75-79] and modified by Chen and Balance [80] can be applied to properly design the controllers in the loop shaping step.

At the same time, arbitrarily picking the wrong order of the loops to be designed can result in the non-existence of a solution. This may occur if the solution process is based on satisfying an upper limit of the phase margin frequency ω_{ϕ}, for each loop. Hence, Loop i having the smallest phase margin frequency will have to be chosen as the first loop to be designed. The loop that has the next smallest phase margin frequency will be next, and so on [4].

It is important to notice that the calculation of the equivalent plant $\left(p_{kk}^{*e}\right)^{-1}$ usually introduces some exact pole-zero cancellations. That operation can be precisely done using symbolic mathematic tools, but could be erroneously done when using numerical calculus due to the typical round errors.

Finally, every step of the proposed methodology can be aided by existing QFT software packages [95-102].

4.0 NON-DIAGONAL MIMO QFT CONTROLLER FOR A SCARA ROBOT [62]

The non-diagonal MIMO QFT controller design technique is applied to control a real-world problem: a SCARA robot [115]. Fig. 12 shows the AdeptOne robot manipulator, and the two joint angles $-\delta_1$ and δ_2- that are considered in this example. In order to present the control of two joints of the SCARA robot, the plant model and the desired performance specifications are introduced in the next sections.

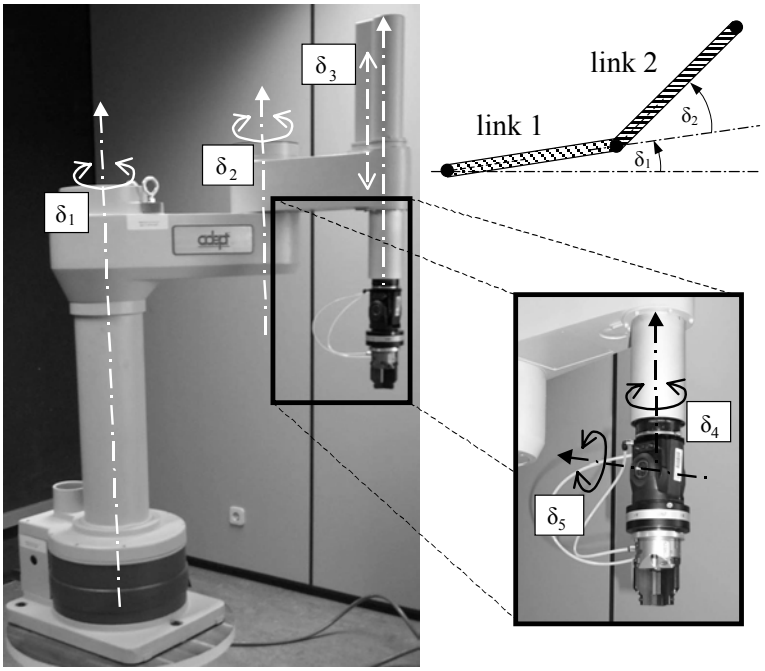

Fig. 12 Adept One SCARA Robot

4.1 Plant Model

The Lagrange equations' method is used to find Eqs. (66) and (67), which describe the non-linear dynamic behaviour of the two-link system [115]. The real inputs are the torques τ_1 and τ_2 -applied through power amplifier as u_1 and u_2- commanded by electrical motors on joints 1 and 2, and the outputs are angles δ_1 and δ_2.

$$\left[\alpha_1 + 2\,\alpha_3\,\cos(\delta_2)\right]\ddot{\delta}_1 + \left[\alpha_2 + \alpha_3\,\cos(\delta_2)\right]\ddot{\delta}_2 + \nu_1\,\dot{\delta}_1 + \mu_1\,\mathrm{sgn}(\dot{\delta}_1) = \tau_1 = \frac{u_1}{k} \qquad \textbf{(66)}$$

$$\left[\alpha_2 + \alpha_3 \cos(\delta_2)\right] \ddot{\delta}_1 + \alpha_2 \ddot{\delta}_2 + \nu_2 \dot{\delta}_1 + \mu_2 \operatorname{sgn}(\dot{\delta}_2) = \tau_2 = \frac{u_2}{k} \tag{67}$$

where k is the power amplifiers' gain, ν_i are coefficients of viscous friction, μ_i Coulomb friction parameters associated with link i, and,

$$\left.\begin{aligned} \alpha_1 &= I_1 + I_2 + m_1 x_1^2 + m_2 \left(l_1^2 + x_2^2\right) \\ \alpha_2 &= I_2 + m_2 x_2^2 \\ \alpha_3 &= m_2 l_1 x_2 \end{aligned}\right\} \tag{68}$$

denoting I_i, m_i and x_i as the moment of inertia, mass and position of the i-th link respectively, and l_1 as the length of link 1.

Input signals u_1 and u_2 will be computed in counts [ct] and will be commanded to the robot motors by the amplifiers. After a robust parameter identification process [115], the coefficients of the robot model, with a uniform Probability Distribution, were found (Table IV).

Table IV: Coefficients of uncertain plant. Uniform Probability Distribution.

	Minimum	Maximum	Nominal
$\alpha_1 \cdot k$ [ct·s^2/rd]	719	813	766
$\alpha_2 \cdot k$ [ct·s^2/rd]	186	200	193
$\alpha_3 \cdot k$ [ct·s^2/rd]	134	230	182
$\nu_1 \cdot k$ [ct·s/rd]	67	381	224
$\nu_2 \cdot k$ [ct·s/rd]	11.6	91.9	51.75
$\mu_1 \cdot k$ [ct]	344	358	351
$\mu_2 \cdot k$ [ct]	262	323	292.5

Now it is possible to consider the Coulomb frictions as disturbances and the cosine value of δ_2 as an uncertain parameter h between -1 and +1. Taking into account Eqs. (66) and (67), it is easy to find the following linear transfer functions, which are the elements of the plant ***P*** defined as,

$$\begin{bmatrix} \delta_1 \\ \delta_2 \end{bmatrix} = P \begin{bmatrix} u_1 \\ u_2 \end{bmatrix} = \begin{bmatrix} p_{11} & p_{12} \\ p_{21} & p_{22} \end{bmatrix} \begin{bmatrix} u_1 \\ u_2 \end{bmatrix} \tag{69}$$

$$p_{11}(s) = \frac{\alpha_2 s + \nu_2}{s \Delta(s)} \frac{1}{k} \tag{70}$$

$$p_{12}(s) = \frac{-(\alpha_2 + \alpha_3 h)}{\Delta(s)} \frac{1}{k} \tag{71}$$

$$p_{21}(s) = \frac{-(\alpha_2 + \alpha_3 h)}{\Delta(s)} \frac{1}{k} \tag{72}$$

$$p_{22}(s) = \frac{(\alpha_1 + 2\,\alpha_3 h)s + \nu_1}{s \Delta(s)} \frac{1}{k} \tag{73}$$

where,

$$\Delta = \eta_2\ s^2 + \eta_1\ s + \eta_0 \tag{74}$$

with the following coefficients,

$$\left.\begin{aligned} \eta_2 &= \alpha_2\ (\alpha_1 + 2\ \alpha_3\ h) - (\alpha_2 + \alpha_3\ h)^2 \\ \eta_1 &= \alpha_2\ \nu_1 + \nu_2\ (\alpha_1 + 2\ \alpha_3\ h) \\ \eta_0 &= \nu_1\ \nu_2 \end{aligned}\right\} \tag{75}$$

4.2 Performance Specifications

The desired performance specifications for the SCARA robot manipulator are the following,

i. Robust Stability. $|t_{ii}(j\omega)| \le 1.2$, for $i = 1,2\ \forall\omega$, involves a lower phase margin of at least 50º and a lower gain margin of at least 1.833 (5.26 dB).
ii. Control effort constraint. Control signals have to be lower than 32767 [ct] for disturbance rejection at plant output of about 20º.
iii. Disturbance rejection at plant input. The maximum allowed error has to be of 30º for torque disturbances of 1000 [ct].
iv. Loop Coupling. Reduction of coupling effect as much as possible.
v. Tracking specifications. $|\boldsymbol{T}_{y/r}(j\omega)|$ has to achieve tracking tolerances defined by,

$$a_{ii}(\omega) \le \left|t_{ii}^{y/r}(j\omega)\right| \le b_{ii}(\omega) \quad \text{for } i = 1,2 \tag{76}$$

where,

$$b_{ii}(\omega) = \left|\frac{12.25\ [(j\omega)/30 + 1]}{(j\omega)^2 + 5.25\ (j\omega) + 12.25}\right| \tag{77}$$

$$a_{ii}(\omega) = \left|\frac{2.25}{\left[(j\omega)^2 + 4.5\ (j\omega) + 2.25\right][(j\omega)/10 + 1]}\right| \tag{78}$$

The above specifications are limited by the achieved sampling time for the practical implementation, which is actually 10 ms.

4.3 Controller Design

- Step A: Coupling analysis and pairing

The first step is the RGA. This analysis yields a very obvious result: angle δ_1 will be controlled by motor 1 (u_1), and angle δ_2 by motor 2 (u_2). The first element λ_{11} plotted in Fig. 13 also shows that the robot arm presents a very coupled behaviour. At low frequencies -below 0.06 rad/s- the coupled behaviour is very low, but as far as the frequency increases the system presents a more coupled dynamics. The required bandwidth of the system derived from tracking specifications lies between approximately 2 and 3.5 rad/s.

In those frequencies the maximum value of λ_{11} is greater than 4.5.

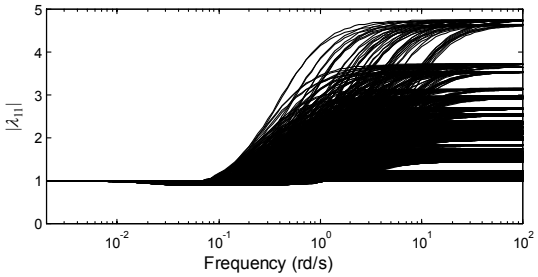

Fig. 13 Element λ_{11} of the Relative Gain Analysis Matrix

- Step B.1: Design of the first loop controller, $g_{11}(s)$.

Taking into account the model uncertainty of $\left(p_{11}^{*}\right)^{-1}$ and the desired specifications for the Loop 1, the controller of Eq. (61) is found, satisfying all the performance specifications -see Fig. 14a-.

$$g_{11}(s) = \frac{1.65\ s^2 + 4.3840\ s + 2.6190}{\left(s^2 + 829.2\ s + 1.545\ 10^5\right) s}\ 10^9 \tag{79}$$

- Step C.1: Design of the decoupling element of control effort u_1 on angle δ_2.

Taking into account the optimum controller for reference tracking problems of Eq. (51), the controller g_{21} of Eq. (80) is designed minimising the coupling effect c_{21}. Fig 14c shows the frequency plot of the obtained coupling reduction.

$$g_{21}(s) = \frac{3860\ s^2 + 10300\ s + 6130}{848\ 10^{-6}\ s^3 + 0.00703\ s^2 + 1.31\ s + 0.346} \tag{80}$$

- Step B.2: Design of the second loop controller, $g_{22}(s)$.

The following equivalent plant $\left(p_{22}^{*e}\right)^{-1}$ derived from Eq. (62) is calculated,

$$\left[p_{22}^{*e}\right]_2 = \left[p_{22}^{*}\right]_1 - \frac{\left(\left[p_{21}^{*}\right]_1 + \left[g_{21}\right]_1\right)\left(\left[p_{12}^{*}\right]_1 + \left[g_{12}\right]_1\right)}{\left[p_{11}^{*}\right]_1 + \left[g_{11}\right]_1} \tag{81}$$

The controller of Eq. (82) is found, satisfying all the performance specifications -see Fig. 14d-.

$$g_{22}(s) = \frac{88.1\ s^2 + 225\ s + 110}{\left(10^{-6}\ s^2 + 0.371\ 10^{-3}\ s + 0.0344\right) s} \tag{82}$$

- Step C.2: Design of the decoupling element of control effort u_2 on angle δ_1.

The controller g_{12} of Eq. (83) is designed minimising the coupling effect c_{12}. Fig 14b shows the frequency plot of the obtained coupling reduction.

$$g_{12}(s) = \frac{20600\ s^2 + 52600\ s + 25700}{0.193 \cdot 10^{-3}\ s^3 + 0.0717\ s^2 + 6.66\ s + 1.78} \quad \textbf{(83)}$$

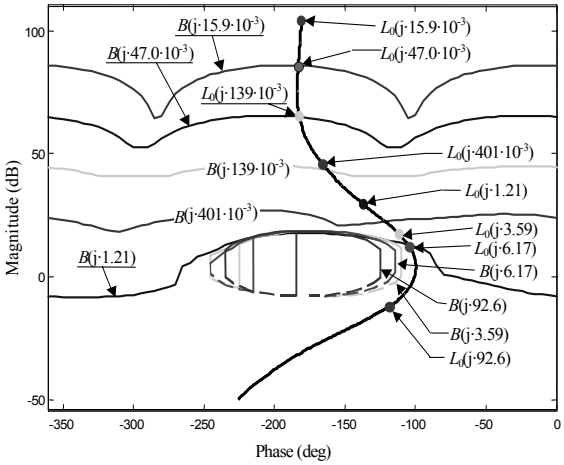

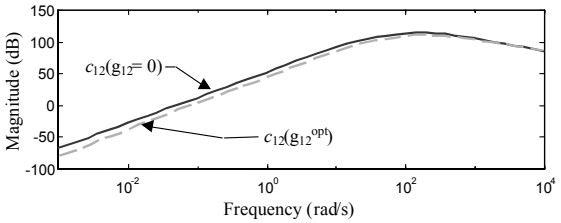

$$L_0(s) = g_{11}(s)\left(p_{11}^*(s)\right)^{-1}$$

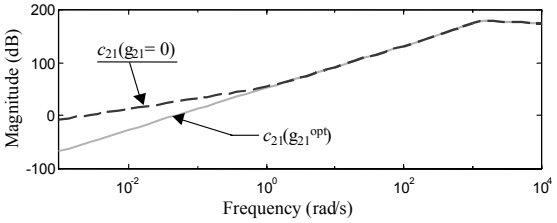

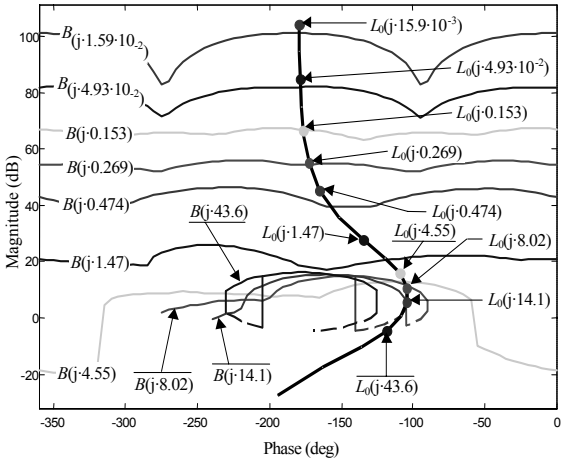

$$L_0(s) = g_{22}(s)\left(p_{22}^{*e}(s)\right)^{-1}$$

Fig. 14 QFT MIMO controller design.

- Step D: Pre-Filters.

Open loop pre-filters of Eq. (84) and Eq. (85) are included in order to satisfy time domain specifications for reference tracking.

$$f_{11}(s) = \frac{14.3}{s^2 + 7.5620\ s + 14.3} \quad \textbf{(84)}$$

$$f_{22}(s) = \frac{3.026}{s^2 + 6.355\, s + 3.026} \tag{85}$$

4.4 Experimental Results

To control the AdeptOne SCARA robot, a digital form of the designed non-diagonal QFT compensator is implemented in a Motorola 68040 microprocessor (25 MHz), with a 8 Mbyte DRAM memory and a VME bus card, and using a sampling time of 10 ms. The two plant outputs, angles δ_1 and δ_2, are measured by encoders, and the two plant inputs, signals u_1 and u_2, are applied to a power amplifier that commands two direct drives that move the arms (see Fig. 15).

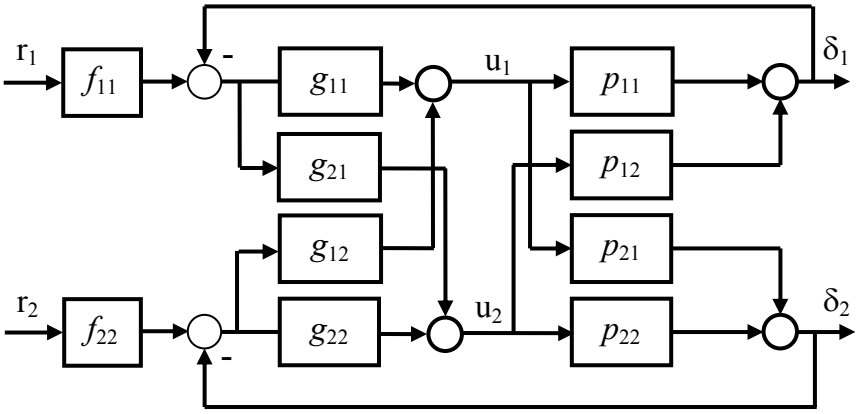

Fig. 15 Block diagram of the control system.

The obtained results with the non-diagonal QFT controller, when the reference r_1 for angle δ_1 is commanded from 0 up to 45 degrees and while the reference r_2 for angle δ_2 is kept constant (zero degrees), are shown in Fig. 16. The same experiment with only the pure diagonal controller is shown in Fig. 17.

Similarly, the results obtained with the non-diagonal QFT controller, when the reference r_2 for angle δ_2 is commanded from 0 up to 45 degrees and while the reference r_1 for angle δ_1 is kept constant (0 degrees), are shown in Fig. 18. The same experiment with only the pure diagonal controller is shown in Fig. 19.

Both real experimental results show how the non-diagonal controller (see Fig. 16 and 18) reach a significative reduction of the coupling effect with respect to the performance of the pure diagonal controller (see Fig. 17 and 19).

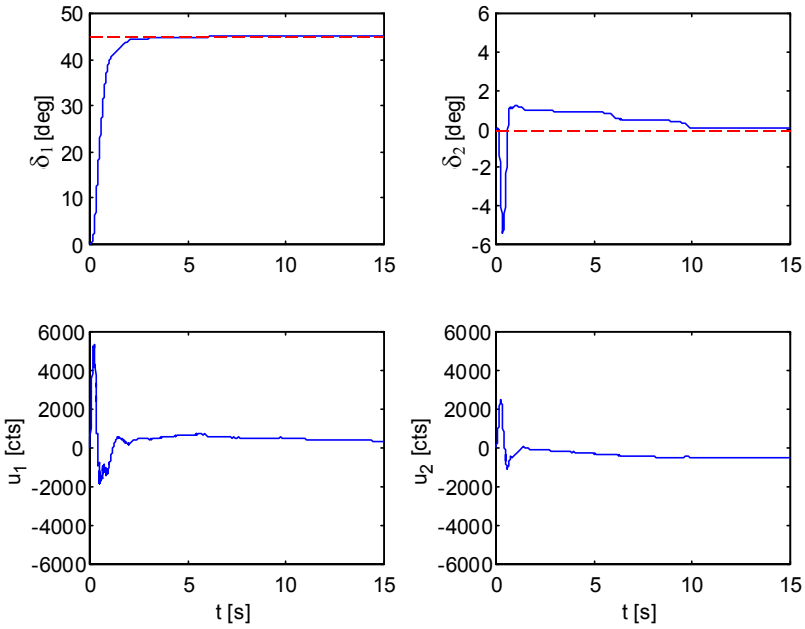

Fig. 16 Step input at r_1 with a fully populated (non-diagonal) matrix controller.

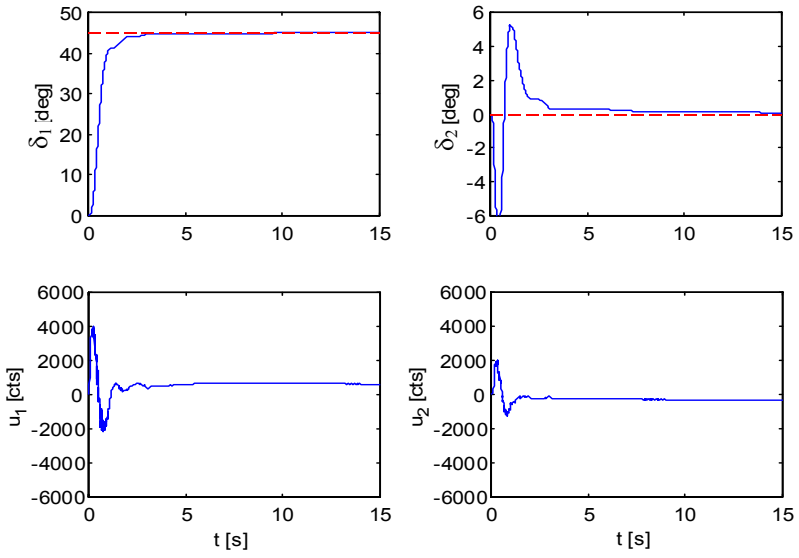

Fig. 17 Step input at r_1 with a pure diagonal matrix controller.

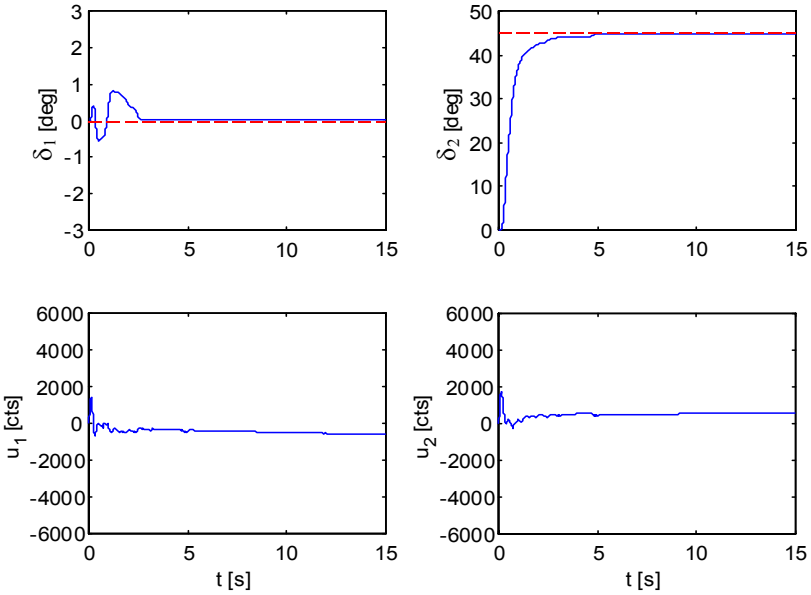

Fig. 18 Step input at r_2 with a fully populated (non-diagonal) matrix controller.

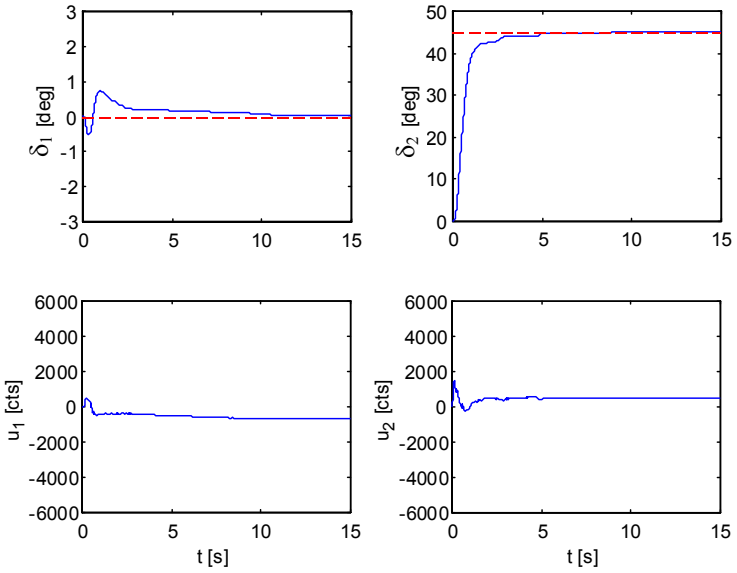

Fig. 19 Step input at r_2 with a pure diagonal matrix controller.

5.0 QFT CONTROL OF A WASTEWATER TREATMENT PLANT [114]

One of the main objectives of a Waste Water Treatment Plant (WWTP) is to protect the water environment from negative effects produced by residual pernicious substances. Figures 20 and 21 show the new activated sludge WWTP of Crispijana, Spain, which is able to regulate both the ammonia and nitrate concentration in the effluent, dealing with water influent of about 5000 m^3/hour.

The control strategies designed to regulate that WWTP were based on a hierarchical structure where a high-level or supervisor selects the set-point of the low-level or conventional controllers. The design of the controllers was carried out using the Quantitative Feedback Theory (QFT).

Nitrate control aims at the optimal use of the de-nitrification potential at any moment. For this purpose, the control algorithm continuously adapts an internal recycle flow in order to maintain a desired nitrate set-point in the anoxic zone (second loop). Ammonia control aims at maintaining the required average concentration of ammonia in the effluent by manipulating the Dissolved Oxygen set-point that commands several air flow turbines (first loop). Mobile average values of some variables were also introduced in order to eliminate the perturbations associated with the daily 24-hours profiles.

The controllers were designed and verified using long-time dynamic simulations based on a multivariable and nonlinear mathematical model (IWA nº 1) previously calibrated with real data measured in the full-scale WWTP during 12 months. The results obtained in the regulation of the pilot plant show a tighter control of the effluent nitrogen compounds and a significant reduction -energy saving- of the dissolved oxygen demand, rejecting the plant disturbances and insuring robust stability.

Fig. 20 Wastewater Treatment Plant of Crispijana, Spain. (Courtesy of AMVISA).

The main control objective of the first loop is to guarantee the standard requirements of ammonia concentration in the plant effluent, fixed on a daily average $\overline{SNH}$ lower than 2 mg/l. Accordingly, the set point is fixed to 1.3 mg/l. The maximum allowed value (saturation limit) of the *DO* variable is 2 mg/l. In Fig. 22 the daily average of the effluent ammonia concentration $\overline{SNH}(t)$ is shown as a dashed line and the control input *DO(t)* is shown as a solid line, both in mg/l, which are obtained with the $G_{11}(z)$ controller, under a typical influent ammonia load and the temperature conditions.

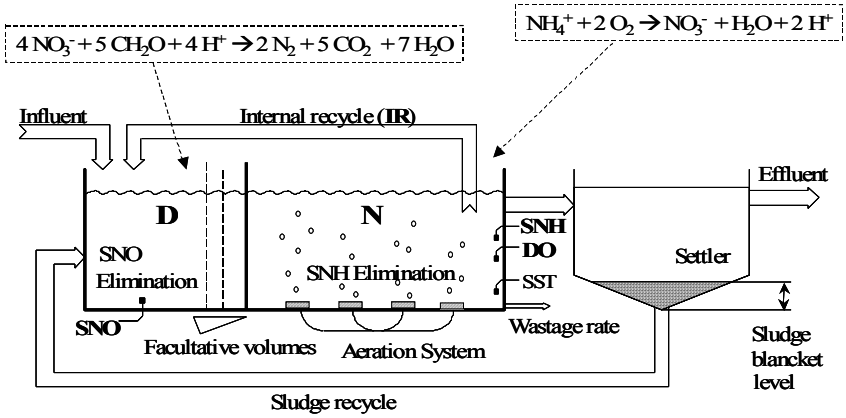

Fig. 21 Wastewater plant diagram (D-N configuration).

Simultaneously, the main control objective of the second loop is to guarantee the standard requirements of nitrates concentration in the plant effluent, fixed on a daily average $\overline{SNO}$ lower than 2 mg/l. For this reason, the controller tries to strengthen the denitrification process in the D tank to minimize the nitrates concentration in the plant effluent. Thus, in the present experiment the set-point of the nitrates concentration in the D tank is fixed to 0.5 mg/l. The maximum allowed value of the *IR* variable is 200% of the design value of the influent flow rate. In Fig. 23 the daily average of the nitrates concentration $\overline{SNO}\,(t)$ is shown in the D tank as a dashed line [mg/l] and the control input $IR(t)$ is shown as a solid line [per unit of the influent flow rate] with the $G_{22}(z)$ controller, under a typical influent ammonia load and the temperature conditions.

Figures 22 and 23 show how the system is able to regulate within the required specifications for both loops, except in the intervals when external disturbances saturate the control inputs:

- First Loop. *DO* saturated: [7→12, 13→14, 16→17, 34→35] days.
- Second Loop. *IR* saturated: [19→24, 29→34] days.

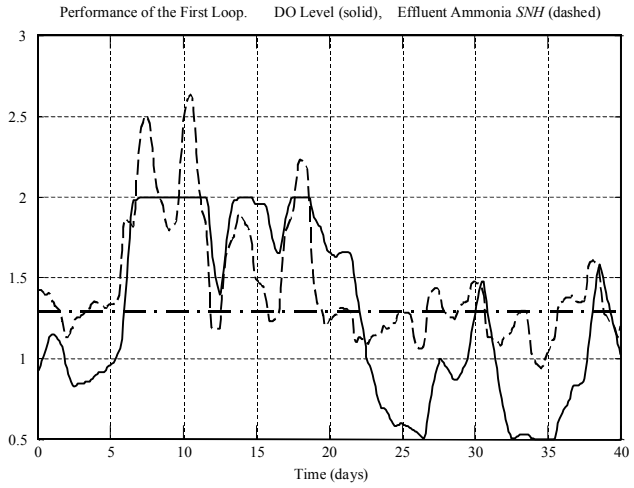

Fig. 22 First loop performance with $G_{11}(z)$.

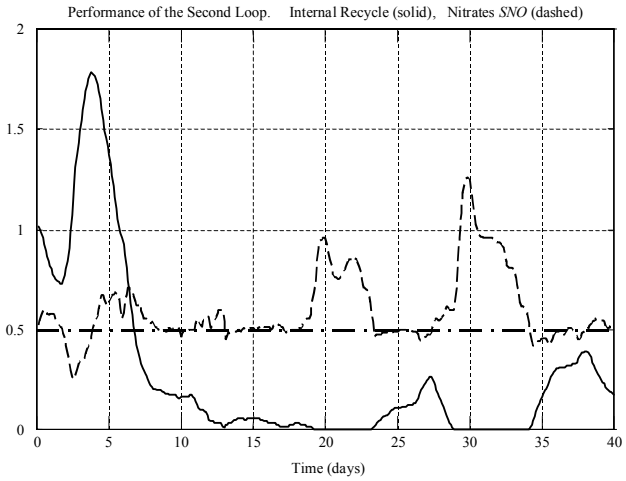

Fig. 23 Second loop performance with $G_{22}(z)$.

In these cases, the system runs in the best possible conditions, obtaining a good performance when the saturation disappears. The control system achieves satisfactory performance of the effluent ammonia and nitrates concentrations over the whole range of operational conditions. It also obtains a notable reduction of the running costs, minimizing the oxygen supplied by the aeration system.

6.0 QFT CONTROL OF A LARGE WIND TURBINE [124, 125]

Large Wind Turbines (WT) present a very complex multi-objective control problem that combine critical reliability issues with non-linear optimization matters. Advanced QFT robust control strategies have been thoroughly applied in the design, development and control of the new real Wind Turbines of 1500 and 1650 kW, made by M.Torres company (Fig. 24). The WTs are a variable speed, pitch controlled, multi-pole synchronous generator with two controlled IGBT's electrical power converters connected to the stator. The main dimensions are about 72 m of rotor diameter (blades of 36 m) and 65 m of tower.

Fig. 24 Multipole Variable Speed Wind Turbine, 1650 kW. (Courtesy of M.Torres)

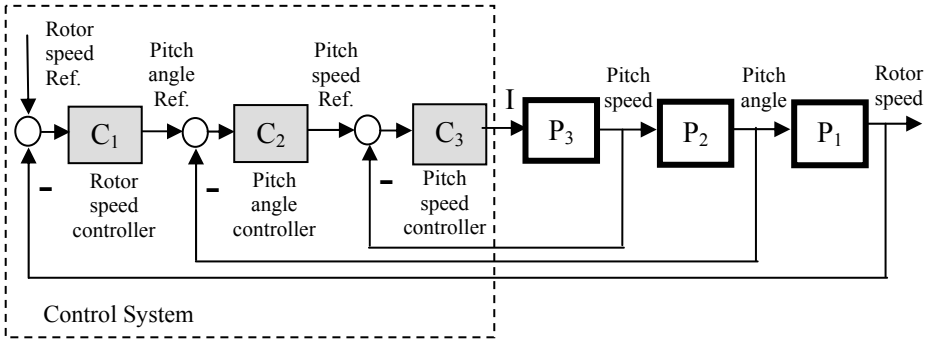

Fig. 25 Rotor speed control system block diagram

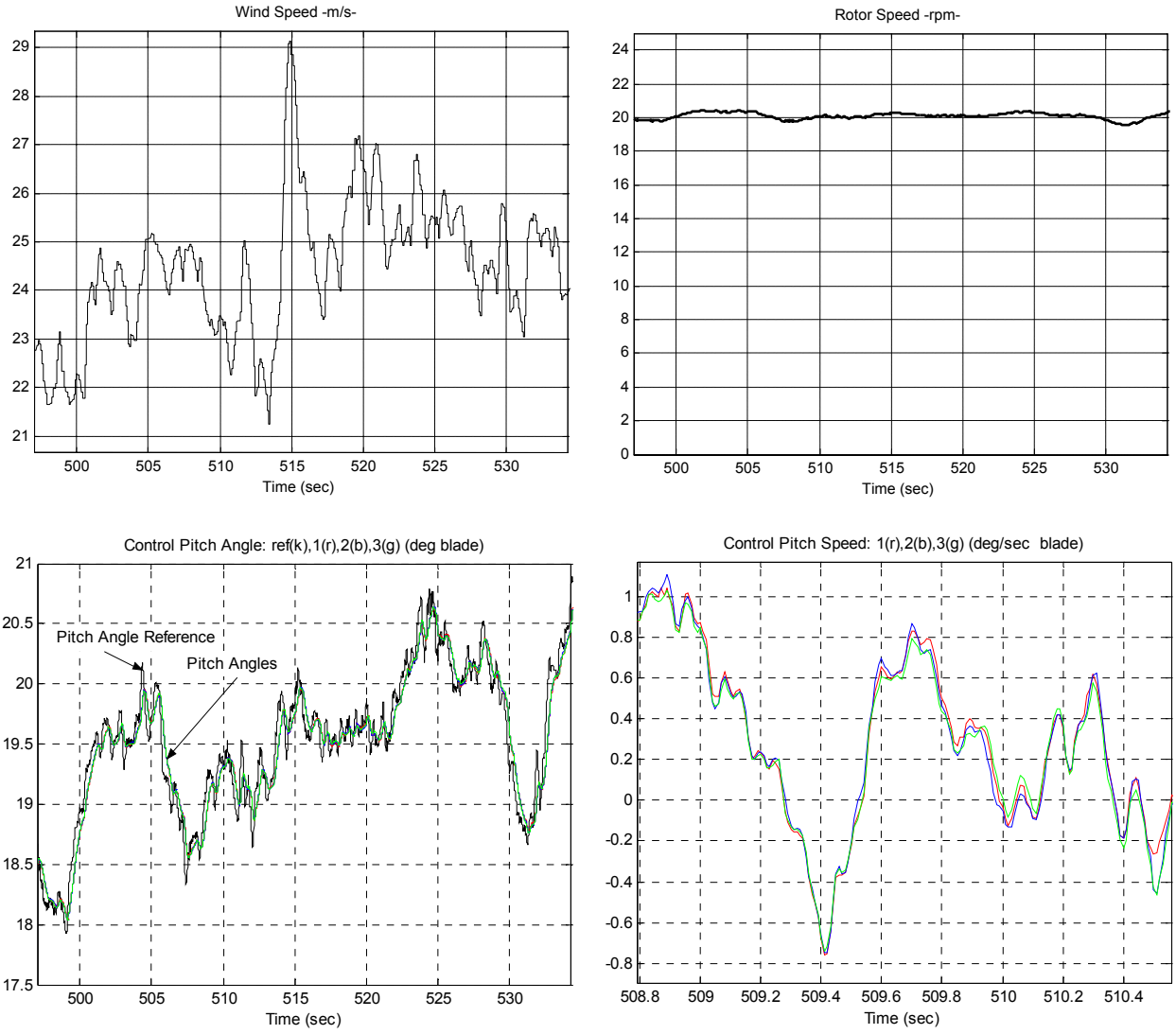

Fig. 26. QFT Control under very high wind speed conditions

The principal targets of the more than 20 loops of the control system cover aspects such as the improvement of the maximum power efficiency for every wind speed, the attenuation of the transient

mechanical loads and fatigue stresses, the reduction of the electrical harmonics and flicker, and the robustness against parameters variation with a redundant fault tolerance system. In addition some critical problems arise in the design of the WT control system, such as the difficulty to work safely with random and extreme gusts, the complexity introduced by the strongly nonlinear, multivariable and time variable mathematical model and the impossibility to have a direct measurement of the wind speed experienced by the turbine, because of the high uncertainty in the anemometer measurement and the strong influence of the blades movement. These set of motivations obliged the control engineer to get involved in the design of every dynamic element of the wind turbine from the very beginning of the project, and to combine advanced control strategies such as QFT robust control techniques, adaptive schemes, multivariable methodology and predictive elements. The actual tests that were carried out in several Wind Turbines, for more than three years, with the proposed QFT control methodologies showed very good behavior of the WT, either in low, medium or high winds and even with the extreme 30 m/s case. Figure 25 shows a simplified block diagram of the rotor speed, pitch angle and pitch speed controllers. Figure 26 shows some experimental results of the TWT1650 with the QFT controllers under very high wind speed conditions.

7.0 NON-DIAGONAL QFT CONTROLLER FOR A 3X3 INDUSTRIAL FURNACE [127]

This section addresses the temperature control of a 3-input (power supplies) 3-output (temperature sensors) industrial furnace used to manufacture large composite pieces (see Fig. 27). Due to the multivariable condition of the process, the strong interaction between the three control loops and the presence of model uncertainties, a sequential design methodology based on Quantitative Feedback Theory (QFT) is proposed to design the controllers. The methodology derives a full matrix compensator that improves reliability, stability and control. It not only copes with furnace model uncertainties but also enhances the reference tracking and the homogeneousness of the composite piece temperature while minimizing the coupling effects among the furnace zones and the operating costs (see Fig. 28).

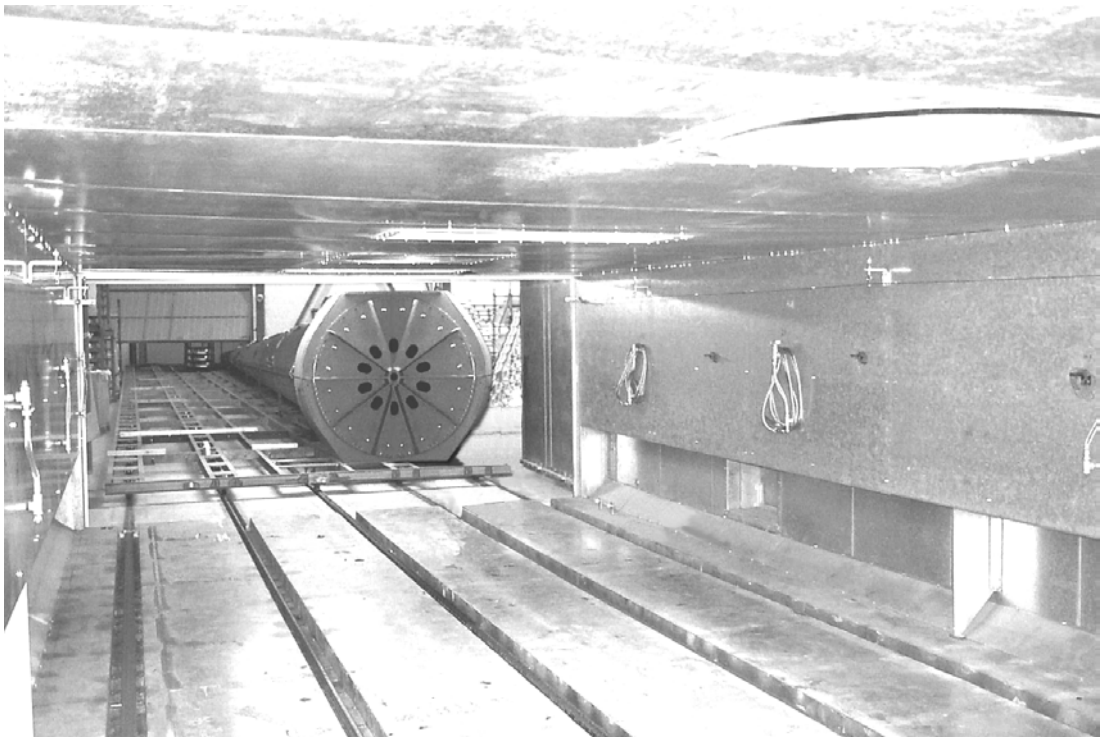

Fig. 27. Industrial furnace and piece to be manufactured inside. (Siflexa, M.Torres-Spain)

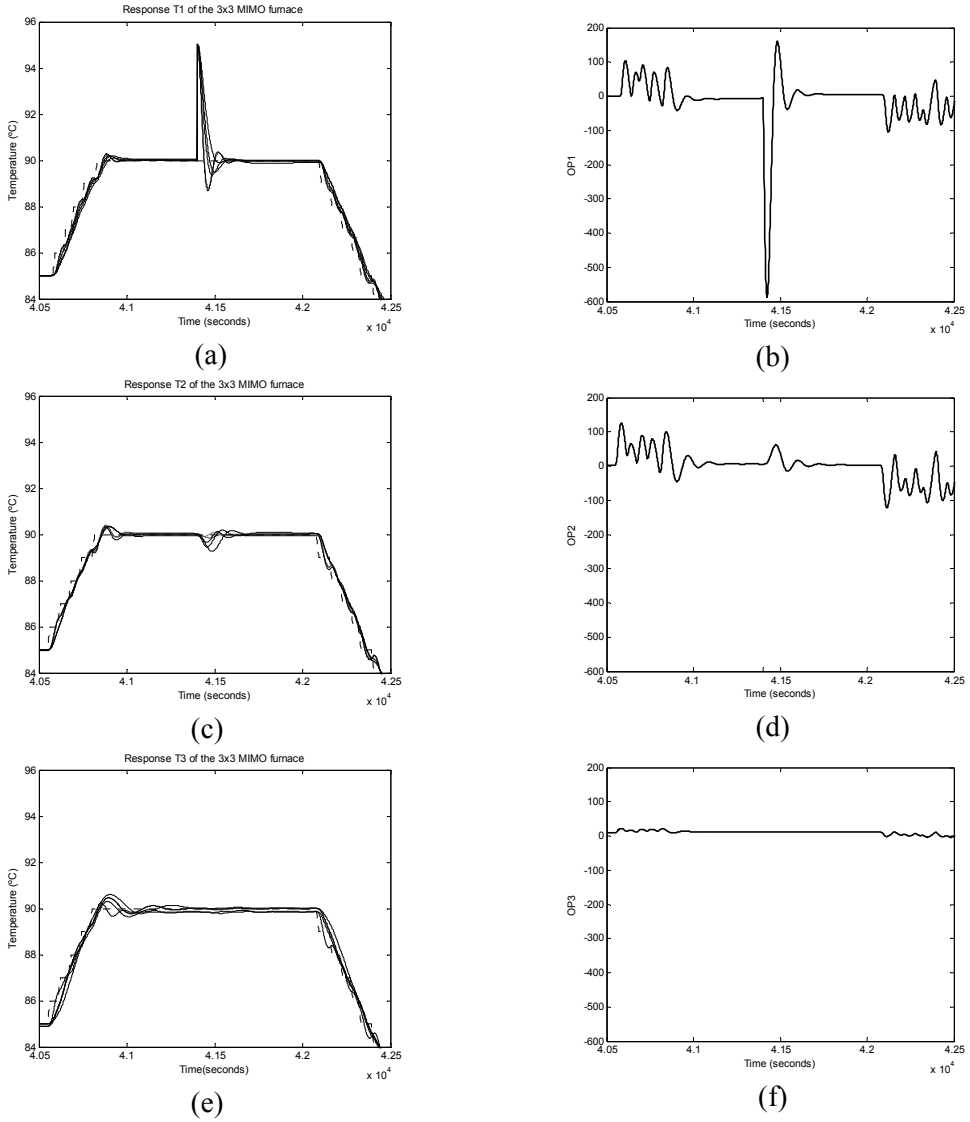

Fig. 28 Response of the 3x3 MIMO industrial furnace, following a reference cure cycle and rejecting a disturbance at plant output in the first channel at t = 41400 sec. (a), (b) T_1 and OP_1. (c), (d) T_2 and OP_2. (e), (f) T_3 and OP_3.

8.0 CONCLUSIONS

Since the very first ideas suggested by Horowitz in 1959 until now, the Quantitative Feedback Theory (QFT) has been successfully applied to many control systems: linear and non-linear, stable and unstable, SISO and MIMO, minimum and non-minimum phase, with time-delay, with lumped and distributed parameters, multi-loop, etc.

The method searches for the controller that guarantees the achievement of the required performance specifications for every plant within the existing model uncertainty. QFT highlights the trade-off (*quantification*) among the simplicity of the controller structure, the minimization of the 'cost of feedback', the quantified model uncertainty and the achievement of the desired performance specifications at every frequency of interest.

The first part of the paper summarized the main concepts of the Quantitative Feedback Theory (QFT) and

presented a wide set of references related to the principal areas of research. The second part of the paper introduced a method to design non-diagonal QFT controllers for MIMO systems. Finally the paper ends presenting some real-world applications of the technique, carried out by the author: an industrial SCARA robot manipulator, a wastewater treatment plant of 5000 m^3/hour, a variable speed pitch controlled multipolar wind turbine of 1.65 MW and an industrial furnace of 40 metres and 1 MW.

ACKNOWLEDGEMENT

The author would like to acknowledge his former PhD students, specially Dr. X.Ostolaza, Dr. J.C. Guillen, Dr. I.Egaña, Dr. M.Gil and Dr. M.Barreras, for their previous collaboration in this work, and wish also to gratefully appreciate the support given by the Spanish "Ministerio de Ciencia y Tecnología" (MCyT) under grant CICYT DPI'2003-08580-C02-01.

REFERENCES

Books

[1]. Bode H.W., (1945), Network Analysis and Feedback Amplifier Design. Van Nostrand Company.

[2]. Horowitz I., (1963), Synthesis of Feedback Systems. New York, Academic Press.

[3]. Horowitz I., (1993), Quantitative Feedback Design Theory (QFT). QFT Pub., 660 South Monaco Parkway, Denver, Colorado 80224-1229.

[4]. Houpis C.H., Rasmussen S.J., Garcia-Sanz, M. (2005), Quantitative Feedback Theory: Fundamentals and Applications. 2ª Edición. CRCPress, Marcel Dekker, NY, USA.

[5]. Yaniv O., (1999), Quantitative Feedback Design of Linear and Non-linear Control Systems. Kluver Academic Pub.

[6]. Sidi M., (2002), Design of Robust Control Systems: From classical to modern practical approaches. Krieger Publishing.

Special Issues about QFT

[7]. Houpis, C.H. (Guest Editor). Quantitative Feedback Theory Special Issue. Int. J. Robust Nonlinear Control. Vol. 7, No. 6, June 1997. Wiley.

[8]. Eitelberg, Eduard (Guest Editor). Isaac Horowitz Special Issue. Int. J. Robust Nonlinear Control. Parte 1, Vol. 11, N. 10, August 2001 and Parte 2, Vol. 12, No. 4, April 2002. Wiley.

[9]. Garcia-Sanz, Mario (Guest Editor). Robust Frequency Domain Special Issue. Int. J. Robust Nonlinear Control. Vol. 13, No. 7, June 2003. Wiley.

International QFT Symposia

[10]. Houpis C.H., and Chander P. (Editors). 1st Int. Symp. on Quantitative Feedback Theory and Robust Frequency Domain Methods, Writght Patterson Airforce Base, Dayton, Ohio, USA, August 1992.

[11]. Nwokah O.D.I., and Chander P. (Editors). 2nd Int. Symp. on Quantitative Feedback Theory and Robust Frequency Domain Methods Purdue University, West Lafayette, Indiana, USA, August 1995.

[12]. Petropoulakis L., and Leithead W.E.(Editors). 3rd Int. Symp. on Quantitative Feedback Theory and Robust Frequency Domain Methods University of Strathclyde, Glasgow, Scotland, UK, August 1997.

[13]. Boje E., and Eitelberg E. (Editors). 4th Int. Symp. on Quantitative Feedback Theory and Robust Frequency Domain Methods University of Natal, Durban, South Africa, August 1999.

[14]. Garcia-Sanz M. (Editor). 5th Int. Symp. on Quantitative Feedback Theory and Robust Frequency Domain Methods Public University of Navarra, Pamplona, Spain, August 2001.

[15]. Boje E., and Eitelberg E. (Editors). 6th Int. Symp. on Quantitative Feedback Theory and Robust Frequency Domain Methods University of Cape Town, Cape Town, South Africa, December 2003.

QFT Tutorials

[16]. Horowitz, I., (1982), Quantitative Feedback Theory. IEE Control Theory and Applications, Vol. 129, pp. 215-226.

[17]. Horowitz, I. (1991), Survey of Quantitative Feedback Theory. International Journal of Control, Vol. 53(2), pp. 255-291.

[18]. Houpis C.H. (1996), Quantitative Feedback Theory (QFT) Technique. en The Control Handbook. CRC Press, IEEE Press. (Editor W.S. Levine), Chapter 44. pp. 701-717.

Comments about history of QFT

[19]. Horowitz, I.M (1992). QFT – Past, present and future. Plenary address. 1st Int. Symp. on QFT and Robust Frequency Domain Methods, Dayton, Ohio, USA, pp. 9-14.

[20]. Horowitz, I.M (1999). Frequency response in control. Plenary. 4th Int. Symp. on QFT and Robust Frequency Domain Methods, Durban, South Africa, pp. 233-239.

[21]. Horowitz, I.M (2002). It was not easy: a personal view. Int. J. Robust Nonlinear Control, Vol. 12, No. 4, pp. 289-293.

[22]. Houpis, C.H. (2002). Horowitz: bridging the gap. Int. J. Robust Nonlinear Control, Vol. 12, No. 4, pp. 293-302.

[23]. Garcia-Sanz, M. (2001). QFT international symposia: past, present and future. Editorial del 5th Int. Symp. on QFT and Robust Frequency Domain Methods, Pamplona, Spain.

First Papers about QFT

[24]. Horowitz I.M, (1959), Fundamental theory of automatic linear feedback control systems. I.R.E. Transactions on Automatic Control, Vol. 4, December, pp. 5-19.

[25]. Horowitz I.M, Sidi M. (1972), Synthesis of feedback systems with large plant ignorance for prescribed time-domain tolerances. Int. J. Control, Vol. 16, No. 2, pp. 287-309.

[26]. Horowitz I.M, (1973), Optimum loop transfer function in single-loop minimum-phase feedback systems. Int. J. Control, Vol. 18, No. 1, pp. 97-113.

[27]. Horowitz, I.M. (1975). A synthesis theory for linear time-varying feedback systems with plant uncertainty. IEEE Transactions on Automatic Control, Vol. AC-20, pp. 454-463.

Papers about QFT Templates

[28]. Bartlett, A.C., Tesi, A., Vicino, A. (1993). Frequency response of uncertain systems with interval plants. IEEE Trans. On Automatic Control, Vol. 38, No. 6, pp. 929-933.

[29]. Bartlett, A.C. (1993). Computation of the frequency response of systems with uncertain parameters: a simplification. Int. J. of Control, Vol. 57, No. 6, 1293-1309.

[30]. Gutman, PO., Baril, C. Neuman, L. (1994), An algorithm for computing value sets of uncertain transfer functions in factored real form. IEEE Trans. on Automatic Control, Vol. 39, No. 6.

[31]. Ballance, D.J., and Hughes, G. (1996), A survey of template generation methods for Quantitative Feedback Theory. UKACC International conference on control '96, pp. 172-174.

[32]. Ballance, D.J., and Chen, W. (1998), Symbolic computation in value sets of plants with uncertain parameters, UKACC International conference on control '98, pp. 1322-1327.

[33]. Garcia-Sanz, M. and Vital P., (1999), Efficient Computation of the Frequency Representation of Uncertain Systems, 4th Int. Symp. on QFT and Robust Frequency Domain Methods, pp. 117-126, Durban, South Africa.

[34]. Nataraj, P.S.V., Sardar, G. (2000). Template generation for continuous transfer functions using interval analysis. Automatica, Vol 36, pp. 111-119.

Papers about QFT Bounds

[35]. Chait Y, and Yaniv O. (1993), Multi-input/single-output computer-aided control design using the Quantitative Feedback Theory. Int. J. Robust Nonlinear Control, 1993, No.3, pp. 47-54.

[36]. Zhao, Y., Jayasuriya, S. (1994). On the generation of QFT bounds for general interval plants. Trans. Of the ASME, Vol. 116, pp. 618-627.

[37]. Rodrigues, J.M., Chait, Y., Yaniv, O. (1997). An efficient algorithm for computing QFT bounds. Trans. of the ASME, Vol. 119, pp. 548-552.

[38]. Moreno, J.C., Baños, A. and Montoya, J.F. (1997). An algorithm for computing QFT múltiple-valued performance bounds. Int. Symp. on QFT and Robust Frequency Domain Methods, pp. 29-34, Scotland.

[39]. Nataraj, P.S.V., Sardar, G. (2000). Computation of QFT bounds for robust sensitivity and gain-phase margin specifications. Trans. of the ASME, Vol. 122, pp. 528-534.

[40]. Nataraj, P.S.V. (2002). Interval QFT: a mathematical and computational enhancement of QFT. Int. J. Robust Nonlinear Control, Vol. 12, No. 4, pp. 385-402.

Papers about QFT Loop-shaping

[41]. Gera, A., Horowitz I.M, (1980), Optimisation of the loop transfer function. Int. J. Control, Vol. 31, No. 2, pp. 389-398.

[42]. Thompson, D.F. and Nwokah, O.D.I. (1994). Analytic loop shaping methods in quantitative feedback theory. ASME, Journal of dynamic systems, measurement and control, Vol. 116, No. 2, pp. 169-177.

[43]. Chait Y., Chen Q., and Hollot C.V. (1997), Automatic loop-shaping of QFT controllers via linear programming, 3rd Int. Symp. on QFT and other Robust Frequency Domain Methods, Glasgow, UK, pp. 13-28.

[44]. Garcia-Sanz, M. and Guillen J.C., (2000), Automatic loop-shaping of QFT robust controllers via genetic algorithms, 3rd IFAC Symposium on Robust Control Design, Praha, Czech Republic.

Papers about existence conditions for QFT controllers

[45]. Nwokah, O.D.I., Thompson, D.F., and Pérez, R.A. (1990). On some existence conditions for QFT controllers, DSC, Vol. 24, pp.1-10.

[46]. Jayasuriya, S. and Y. Zhao, (1994), Stability of Quantitative Feedback Designs and the Existence of Robust QFT Controllers, Int. J. Robust Nonlinear Control. Vol. 4, No. 1, pp. 21-46.

[47]. Gil-Martinez, M. and Garcia-Sanz M., (2003) Simultaneous Meeting of Robust Control Specifications in QFT, Int. J. Robust Nonlinear Control. Vol. 13, No. 7, pp. 643-656.

Papers about QFT for MIMO Systems

[48]. Horowitz I.M, (1979), Quantitative synthesis of uncertain multiple input-output feedback systems. Int. J. Control, Vol. 30, No. 1, pp. 81-106.

[49]. Horowitz I.M, Sidi M., (1980), Practical Design of feedback systems with uncertain multivariable plants. Int. J. Control, Vol. 11, No. 7, pp. 851-875.

[50]. Horowitz, I. M. and C. Loecher, (1981). Design 3x3 Multivariable Feedback System with Large Plant Uncertainty. Int. J. Control. Vol. 33, pp. 677-699.

[51]. Horowitz, I., Neumann, L. and Yaniv, O., (1981). A synthesis technique for highly uncertain interacting multivariable flight control system (TYF16CCV). Proc. Naecon Conf. Dayton, Oh, pp. 1276-1283.

[52]. Horowitz I. (1982). Improved design technique for uncertain multiple input-output feedback systems. Int. J. Control. Vol. 36, pp. 977-988.

[53]. Nwokah, O.D.I., (1984), Synthesis of Controllers for Uncertain Multivariable Plants for Described Time Domain Tolerances, Int. J. of Control, Vol. 40, pp. 1189-1206.

[54]. Yaniv, O., and Horowitz, I.M. (1986). A Quantitative Design Method for MIMO Linear Feedback Systems Having Uncertain Plants, Int. J. of Control, Vol. 43, pp. 401-421.

[55]. Nwokah, O.D.I., (1988), Strong Robustness in Uncertain Multivariable Systems, IEEE Conf. on Decision and Control, Austin, TX.

[56]. Franchek, M.A. and Nwokah O.D.I., (1995), Robust multivariable control of distillation columns using non-diagonal controller matrix, DSC-Vol. 57-1, IMECE, ASME Dynamics systems and control division, pp. 257-264.

[57]. Yaniv, O., (1995), MIMO QFT using non-diagonal controllers, Int. J. of Control, Vol.61, No. 1, pp. 245-253.

[58]. Franchek, M.A, Herman, P. and Nwokah, O.D.I. (1997). Robust nondiagonal controller design for uncertain multivariable regulating systems, ASME J. Dynamic Systems, Measurement and Control, Vol. 119, pp. 80-85.

[59]. Boje, E. (2002). Non-diagonal controllers in MIMO quantitative feedback design. Int. J. Robust Nonlinear Control, Vol. 12, No. 4, pp. 303-320.

[60]. Garcia-Sanz M. and Egaña I. (2002). Quantitative Non-diagonal Controller Design for Multivariable Systems with Uncertainty. Int. J. Robust Nonlinear Control, Vol. 12, No. 4, pp. 321-333.

[61]. De Bedout, J.M. and Franchek M.A., (2002), Stability conditions for the sequential design of non-diagonal mu1tivariable feedback controllers, Int. J. of Control, Vol. 75, N. 12, pp. 910-922.

[62]. Garcia-Sanz M., Egaña I., Barreras M. (2005). Design of QFT Non-Diagonal Controllers for Reference Tracking and External Disturbances Rejection in Uncertain MIMO Systems. Accepted for publication, IEE Control Theory and Applications.

[63]. Kerr, M.L., Jayasuriya S. and Asokanthan S.F, (2005), On stability in non-sequential MIMO QFT designs, accepted for publication, ASME J. Dynamic Systems, Measured and Control.

Papers about QFT for Systems with Long Time-delays

[64]. Garcia-Sanz, M. and Guillen, J.C. (1999) Smith Predictor For Uncertain Systems In The QFT Framework. Lecture Notes in Control and Information Sciences, Ed. Springer Verlag. Vol 243. Progress in System and Robot Analysis and Control Design. Chapter 20, pp. 243-250.

Papers about Digital QFT

[65]. Horowitz, I.M. and Liao, Y. (1986). Quantitative feedback design for sampled-data systems. Int. J. Control, Vol. 44, pp. 665-675.

[66]. Houpis, C.H., and Lamont, B.G. (1992). Discrete quantitative feedback technique, Capítulo 16 en el libro: Digital Control Systems: theory, hardware, software, 2ª edicion. McGraw Hill.

Papers about QFT for Distributed Parameters Systems

[67]. Horowitz, I., Azor, R.. (1983). Quantitative synthesis of feedback systems with distributed uncertain plants. Int. J. Control, Vol. 38, No. 2, pp. 381-400.

[68]. Horowitz, I., Azor, R.. (1984). Uncertain partially non-casual distributed feedback systems. Int. J. Control, Vol. 40, No. 5, pp. 989-1002.

[69]. Horowitz, I., Kannai, Y. and Kelemen, M. (1989). QFT approach to distributed systems Control and Applications. Proceedings ICCON '89. IEEE Int. Conf., pp. 516-519.

[70]. Kelemen M, Kanai Y. and Horowitz I.M. (1989). One-point Feedback Approach to Distributed Linear Systems. Int. Journal of Control , Vol. 49, No. 3, pp. 969-980

[71]. Chait Y, Maccluer C.R. and Radcliffe C.J. (1989). A Nyquist Stability Criterion for Distributed Parameter Systems. IEEE Transactions on Automatic Control, Vol. 34, No. 1, pp. 90-92.

[72]. Kelemen M, Kanai Y. and Horowitz I.M. (1990). Improved method for designing linear distributed feedback systems. Int. Journal of Adaptive Control and Signal Processing, Vol. 4, pp. 249-257.

[73]. Hegde, M.D., Nataraj, P.S.V. (1995). The two-point feedback approach to linear distributed systems. Proc. Int. Conf. On Automatic Control, Indore, India, December 1995.

[74]. Garcia-Sanz, M., Huarte, A. and Asenjo, A. (2005) One-point feedback robust control for distributes parameter systems. Aceptado en IFAC World Congress, Praga.

Papers about QFT for Non-minimum Phase Systems

[75]. Horowitz I.M, Sidi M., (1978), Optimum synthesis of non-minimum phase systems with plant uncertainty. Int. J. Control, Vol. 27, No. 3, pp. 361-386.

[76]. Horowitz I.M, (1979), Design of feedback systems with non-minimum phase unstable plants. Int. J. Systems Science, Vo. 10, pp. 1025-1040.

[77]. Horowitz, I.M. and Liao, Y. (1984). Limitations on non-minimum phase feedback systems. Int. J. Control, Vol. 40, No. 5, pp. 1003-1015.

[78]. Horowitz, I.M., Oldak, S., and Yaniv, O. (1986). An important property of non-minimum phase multi-inputs multi-outputs feedback systems. Int. J. Control, Vol. 44, No. 3, pp. 677-688.

[79]. Horowitz, I.M. (1986). The singular-G method for unstable non-minimum phase plants. Int. J. Control, Vol. 44, No. 2, pp. 533-541.

[80]. Chen, W., Ballance, D. (1998). QFT design for uncertain non-minimum phase and unstable plants. American Control Conference, pp. 2486-2490. Philadelphia, Pennsylvania.

Papers about QFT for Multi-loop Systems

[81]. Horowitz, I.M., Neumann, L. and Yaniv, O. (1985). Quantitative synthesis of uncertain cascade multi-input multi-output feedback systems. Int. J. Control, Vol. 42, No. 2, pp. 273-303.

[82]. Horowitz, I.M., and Yaniv, O. (1985). Quantitative cascade multi-input multi-output symthesis by an improved method. Int. J. Control, Vol. 42, No. 2, pp. 305-331.

[83]. Eitelberg, E. (1999). Load Sharing Control. NOYB Press. Durban, South Africa.

Papers about QFT for Non-linear Systems

[84]. Horowitz I.M, (1976), Synthesis of feedback systems with non-linear time-varying uncertain plants to satisfy quantitative performance specifications. IEEE Proc.,Vol.64, pp.123-130.

[85]. Horowitz I.M, (1981), Quantitative synthesis of uncertain non-linear feedback systems with non-minimum phase inputs. Int. J. Systems Science, Vol. 1, No. 12, pp. 55-76.

[86]. Horowitz, I.M., (1981). Improvements in quantitative non-linear feedback design by cancelation. Int. J. Control, Vol. 34, No. 3, pp. 547-560.

[87]. Horowitz, I.M., (1982). Feedback systems with non-linear uncertain plants. Int. J. Control, Vol. 36, pp. 155-171.

[88]. Horowitz, I.M., (1983). A synthesis theory for a class of saturating systems. Int. J. Control, Vol. 38, No. 1, pp. 169-187.

[89]. Horowitz, I.M., and Liao, Y., (1986). Quantitative non-linear compensation design for saturating unstable uncertain plants. Int. J. Control, Vol. 44, pp. 1137-1146.

[90]. Oldak S., Baril C. and Gutman P.O., (1994). Quantitative design of a class of nonlinear systems with parameter uncertainty. Int. J. Robust Nonlinear Control, Vol. 4, pp. 101-117.

[91]. Baños, A. and Barreiro, A. (2000). Stability of non-linear QFT designs based on robust absolute stability criteria. Int. Journal of Control, Vol. 73, No. 1, pp. 74-88.

[92]. Baños, A., Barreiro, A., Gordillo, F. and Aracil, J. (2002). A QFT framework for nonlinear robust stability. Int. J. Robust Nonlinear Control, Vol. 12, No. 4, pp. 357-372.

Papers about QFT for LTV Systems

[93]. Yaniv. O., Boneh, R. (1997). Robust LTV feedback synthesis for SISO nonlinear plants. Int. J. of Robust and Nonlinear Control, Vol. 7, pp. 11-28.

[94]. Yaniv. O. (1999). Robust LTV feedback synthesis for nonlinear MIMO plants. Trans. of the ASME Vol. 121, pp. 226-232.

QFT Software Packages

[95]. Sating, R.R., (1992). Development of an Analog MIMO Quantitative Feedback Theory (QFT) CAD Package, MS Thesis, AFIT/GE/ENG/92J-04, Air Force Institute of Technology, Wright Patterson AFB, OH.

[96]. Sating, R.R., Horowitz, I.M. and Houpis, C.H. (1993). Development of a MIMO QFT CAD Package (Ver.2), Air Force Institute of Technology, Wright-Patterson AFB, OH 45433, USA, American Control Conference.

[97]. Houpis, C.H., Sating, R.R., (1997). MIMO QFT CAD Package (Ver.3), Int. J. Control, Vol. 7, No. 6, pp. 533-549.

[98]. Borghesani, C., Chait, Y. and Yaniv, O., (1994, 2002). Quantitative Feedback Theory Toolbox – For use with MATLAB. Terasoft.

[99]. Gutman P-O., (1996). Qsyn - the Toolbox for Robust Control Systems Design for use with Matlab, User's manual, NovoSyn AB, Jonstortpsvagen 61, Jonstorp, Sweden.

[100]. Houpis C.H., Rasmussen S.J., Garcia-Sanz, M. (2001, 2005), Software de diseño del libro Quantitative Feedback Theory: Fundamentals and Applications. Edición 2ª. CRCPress, Marcel Dekker: NY, USA.

[101]. Garcia-Sanz, M., Vital P., Barreras M., and Huarte A. (2001, 2004). InterQFT. Public University of Navarra. También presentado como Interactive Tool for Easy Robust Control Design, IFAC Int. Workshop on Internet Based Control Education, pp. 83-88, Madrid, Spain.

[102]. Diaz J.M., Dormido S., and Aranda J. (2004), SISO-QFTIT, una herramienta software interactiva para diseño de controladores robustos usando QFT. UNED, Madrid, Spain.

Real-world QFT Applications

[103]. Horowitz, I.M. et al, (1982). Multivariable Flight Control Design with Uncertain Parameters (YF16CCV), AFWAL-TR-83-3036, Air Force Wright Aeronautical Laboratories, Wright-Patterson AFB, OH.

[104]. Walke, J., Horowitz, I. and Houpis, C. (1984). Quantitative synthesis of highly uncertain MIMO flight control system for the forward swept wing X-29 aircraft. Proc. IEEE Naecon Conf., pp. 576-583.

[105]. Bossert, D.E., (1989). Design of Pseudo-Continuous-Time Quantitative Feedback Theory Robot Controllers, AFIT/GE/ENG/ 89D-2, Air Force Institute of Technology, Wright-Patterson AFB, OH.

[106]. Chait, Y. and Yaniv, O., (1991). Disturbance rejection in flexible structures via the quantitative feedback theory. Dynamics and control of large structures: Proceedings of the 8th VPI & SU Symposium, pp. 445-446.

[107]. Trosen, D.W., (1993). Development of an Prototype Refueling Automatic Flight Control System Using Quantitative Feedback Theory, AFIT/GE/ENG/93-J-03, Air Force Institute of Technology, Wright-Patterson AFB, OH.

[108]. Kelemen, M., and Bagchi, A. (1993). Modeling and feedback control of a flexible arm of a robot for prescribed frequency domain tolerances. Automatica, Vol. 29, pp. 899-909.

[109]. Reynolds, O.R., Pachter, M. and Houpis, C.H. (1994). Design of a Subsonic Flight Control System for the Vista F-16 Using Quantitative Feedback Theory, Proceedings of the American Control Conference, pp. 350-354.

[110]. Rasmussen, S.J. and Houpis, C.H. (1994). Development Implementation and Flight of a MIMO Digital Flight Control System for an Unmanned Research Vehicle Using Quantitative Feedback Theory, Proceedings of the ASME Dynamic Systems and Control, Winter Annual Meeting of ASME, Chicago, IL.

[111]. Osmon, C., Pachter, M. and Houpis, C.H. (1996). Active Flexible Wing Control Using QFT, IFAC 13th World Congress, Vol. H, pp. 315-320, San Francisco, CA.

[112]. Franchek, M. and Hamilton, G.K. (1997). Robust Controller Design and Experimental Verification of I.C. Engine Speed Control, Int. J. of Robust and Nonlinear Control, vol. 7, pp. 609-628.

[113]. Pachter, M., Houpis, C.H. and Kang, K. (1997). Modelling and Control of an Electro-hydrostatic Actuator, Int. J. of Robust and Nonlinear Control, vol. 7, pp. 591-608.

[114]. Garcia-Sanz, M. and Ostolaza J.X., (2000). QFT-Control of a Biological Reactor for Simultaneous Ammonia and Nitrates Removal. Int. J. on Systems, Analysis, Modelling, Simulation, SAMS, No. 36, pp. 353-370.

[115]. Egaña, I., Villanueva, J., and Garcia-Sanz, M. (2001). Quantitative Multivariable Feedback Design for a SCARA Robot Arm, 5th Int. Symp. on QFT and Robust Frequency Domain Methods, pp. 67-72, Pamplona, Spain.

[116]. Kelemen M. and Akhrif O. (2001) Linear QFT control of a highly nonlinear multi-machine power system. Int. J. Robust Nonlinear Control, Vol. 11, No. 10, pp. 961-976.

[117]. Bentley A.E. (2001). Pointing control design for high precision flight telescope using quantitative feedback theory. Int. J. Robust Nonlinear Control, Vol. 11, No. 10, pp. 923-960.

[118]. Liberzon, A., Rubinstein, D, and Gutman, P.O. (2001). Active suspension for single wheel statin of on-road track vehicle. Int. J. Robust Nonlinear Control, Vol. 11, No. 10, pp. 977-999.

[119]. Garcia-Sanz, M., Guillen, J.C., e Ibarrola, J.J. (2001). Robust controller design for time delay systems with application to a pasteurisation process. Control Engineering Practice, No. 9, pp. 961-972.

[120]. Rueda, T.M., Velasco F.J. (2001) Robust QFT controller for marine course-changing control. 5th Int. Symp. on QFT and Robust Frequency Domain Methods, pp. 79-84, Pamplona, Spain.

[121]. Yaniv O., Fried O., and Furst-Yust M. (2002). QFT application for headphone's active noise cancellation. Int. J. Robust Nonlinear Control, Vol. 12, No. 4, pp. 373-383.

[122]. Gutman, P.O., Horesh, E., Guetta, R., and Borshchevsky, M. (2003). Control of the Aero-Electric Power Station – an exciting QFT application for the 21st century. Int. J. of Robust and Nonlinear Control, Vol. 13, No. 7, pp. 619-636.

[123]. Torres E., and Garcia-Sanz M. (2004), Experimental Results of the Variable Speed, Direct Drive Multipole Synchronous Wind Turbine: TWT1650. Wind Energy, Vol. 7, Num 2, pp. 109-118, Wiley.

[124]. Garcia-Sanz, M. and Torres E., (2004), Control y experimentación del aerogenerador síncrono multipolar de velocidad variable TWT1650, RIAI, Vol. 1, No. 3, pp. 53-62.

[125]. Garcia-Sanz, M. and Hadaegh, FY. (2004). Coordinated Load Sharing QFT Control of Formation Flying Spacecrafts. 3D Deep Space and Low Earth Keplerian Orbit problems with model uncertainty, NASA-JPL, JPL Document, D-30052, Pasadena, California, USA.

[126]. Kerr, M., (2004). Robust Control of an Articulating Flexible Structure Using MIMO QFT, PhD. Dissertation, The University of Queensland, Australia.

[127]. Garcia-Sanz, M. and Barreras, M. (2005). Non-diagonal QFT controller design for a 3-input 3-output industrial Furnace. Sent to the International Journal of Heat and Mass Transfer, Elsevier, The Netherlands.

Miscellaneous

[128]. Rosenbrock HH. (1970). State Space and Multivariable Theory. London: Nelson.

[129]. O'Reilly J. (1987). Multivariable control for industrial applications. IEE, Vol. 32, Peter Peregrinus Ltd., London.

[130]. Maciejowski J.M. (1989). Multivariable feedback design, Addison Wesley, Harlow, United Kingdom.

[131]. Skogestad S., Postlethwaite I. (1996). Multivariable Feedback Control. Wiley.

[132]. Marlin ET. (1995). Process Control: Designing Processes and Control Systems for Dynamic Performance. McGraw-Hill: New York.

[133]. Leithead WE, O'Reilly J. (1992). m-Input m-output feedback control by individual channel design. Part 1. Structural issues. International Journal of Control, Vol. 56 (6), pp. 1347-1397.

[134]. Bristol EH. (1966). On a new measure of interactions for multivariable process control. Transactions on Automatic Control, Vol. 11, pp. 133-134.

[135]. Skogestad S, Havre K. (1996). The use of RGA and condition number as robustness measures. Proceedings of the European Symposium of Computer-Aided Process Engineering; Rhodes, Greece.